CHAPTER THREE

In situ absorbance measurements: a new means to study respiratory electron transfer in chemolithotrophic microorganisms

Robert C. Blake II[a,*] **and Richard A. White III**[b,c,d]

[a]College of Pharmacy, Xavier University of Louisiana, New Orleans, United States
[b]Department of Plant Pathology, Washington State University, Pullman, WA, United States
[c]RAW Molecular Systems (RMS) LLC, Spokane, WA, United States
[d]Australian Centre for Astrobiology, University of New South Wales, Sydney, NSW, Australia
*Corresponding author: E-mail: rblake@xula.edu

Contents

Abstract

Absorbance measurements on intact chemolithotrophic microorganisms that respire aerobically on soluble iron are described that used a novel integrating cavity absorption meter to eliminate the effects of light scattering on the experimental results. Steady state kinetic measurements on ferric iron production by intact cells revealed that the Michaelis Menten equation described the initial rates of product formation for at least 8 different chemolithotrophic microorganisms in 6 phyla distributed equally among the archaea and the Gram negative and Gram positive eubacteria. Cell-monitored turnover

Advances in Microbial Physiology, Volume 76
ISSN 0065-2911
https://doi.org/10.1016/bs.ampbs.2020.01.003

measurements during aerobic respiration on soluble iron by the same 12 intact microorganisms revealed six different patterns of iron-dependent absorbance changes, suggesting that there may be at least six different sets of prosthetic groups and biomolecules that can accomplish aerobic respiration on soluble iron. Detailed kinetic studies revealed that the 3-component iron respiratory chain of *Acidithiobacillus ferrooxidans* functioned as an ensemble with a single macroscopic rate constant when the iron-reduced proteins were oxidized in the presence of excess molecular oxygen. The principal member of this 3-component system was a cupredoxin called rusticyanin that was present in the periplasm of *At. ferrooxidans* at an approximate concentration of 350 mg/mL, an observation that provides new insights into the crowded environments in the periplasms of Gram negative eubacteria that conduct electrons across their periplasm. The ability to conduct direct spectrophotometric measurements under noninvasive physiological conditions represents a new and powerful approach to examine the rates and extents of biological events *in situ* without disrupting the complexity of the live cellular environment.

Abbreviations

Ah	Acidihalobacter
Ali	Alicyclobacillus
Am	Acidimicrobium
Ap.	Acidiplasma
At	Acidithiobacillus
Fm	Ferrimicrobium
Fp.	Ferroplasma
ICAM	Integrating Cavity Absorption Meter
L.	Leptospirillum
M	Metallosphaera
S	Sulfolobus
Sb	Sulfobacillus
tBLASTn	translation Basic Local Alignment Search Tool nucleotide

1. Introduction

Certain chemolithotrophic microorganisms inhabit the immediate vicinity of geological formations and thrive at the expense of exchanging electrons with inorganic minerals within an ore body. Aerobic microorganisms accept/extract electrons from reduced minerals that can be oxidized and conduct respiratory electron transport and oxidative phosphorylation to obtain biochemical energy for growth by passing those electrons to molecular oxygen as the terminal electron acceptor. Under anoxic conditions, certain iron-oxidizing microorganisms can also utilize nitrate, chlorate, or perchlorate as alternative terminal electron acceptors. Anaerobic

microorganisms exploit oxidized minerals as an electron sink to rid themselves of the excess electrons derived from the catabolic oxidation of reduced organic molecules. Both activities/lifestyles have been thoroughly summarized in those cases where the minerals in question contain iron (Weber, Achenbach, & Coates, 2006).

This chapter focuses on the former microorganisms, those that thrive at the expense of oxidizing and solubilizing reduced metal-sulfide minerals like pyrite, FeS_2. The overall oxidation of pyrite in air occurs with the following stoichiometries:

$$2FeS_2 + 7.5O_2 + H_2O \rightarrow Fe_2(SO_4)_3 + {SO_4}^{2-} + 2H^+ \quad (1)$$

$$Fe_2(SO_4)_3 + 6H_2O \rightarrow 2Fe(OH)_3 + 3{SO_4}^{2-} + 6H^+ \quad (2)$$

These aerobic reactions thus produce excess acid, and consequently the microorganisms that catalyze these reactions are both acidogenic and obligately acidophilic. On the one hand, these activities are responsible for the chronic acid pollution that issues from both surface and underground mining operations. On the other hand, these same activities can be exploited for the extraction of metal ions for commercial gain, a process known as bioleaching. The reader is referred elsewhere for reviews that focus on the practical aspects and consequences of these microbial activities (Rawlings, 2002; Vera, Schippers, & Sand, 2013; Watling, 2006).

Oxidation of the sulfide component of pyrite and related minerals is a multi-step process whereby 8 total electrons are available from the transformation of sulfide in its reduced 2- oxidation state to sulfur in its 6+ oxidation state in sulfuric acid. Studies on the dissimilatory oxidation of reduced sulfur are greatly complicated by the facile reactivities of the partially reduced/oxidized intermediary forms of inorganic sulfur metabolites, particularly under the extreme acidic conditions ($pH < 3$) that are typically present in bioleaching environments. The complex chemistry of partially oxidized/reduced inorganic sulfur compounds is summarized in the older literature (Harrison, 1984, and references therein). Mechanistic studies on the enzymology and physiology of dissimilatory sulfur oxidation by microorganisms is an ongoing topic (Ghosh & Dam, 2009; Grabarczyk & Berks, 2017; Watanabe et al., 2019) that is beyond the scope of this chapter.

This chapter summarizes the *in situ* studies of the electron transfer proteins that participate in aerobic respiration on soluble iron under strongly acidic conditions. As has been thoroughly reviewed by Ingledew and his collaborators over the years (Alexander, Leach, & Ingledew, 1987;

Ingledew, 1982; Ingledew & Cobley, 1980), the thermodynamic and chemiosmotic constraints that are imposed on a microorganism that conducts aerobic respiration on soluble iron are relatively severe. The standard reduction potential of soluble ionic iron in sulfate media at pH 2.0 is between 650 and 750 mV versus the standard hydrogen electrode, depending on the concentration of sulfate ion (Blake & Shute, 1987). Sulfate binds more strongly to ferric ion than it binds to ferrous ion; consequently higher levels of sulfate lower the reduction potential of the soluble iron, which renders the iron more reducing. The corresponding reduction potential for the oxygen/water couple is on the order of 1120 mV at pH 2.0. That means that approximately 350 mV, or 8.1 kcal/mol, are available from aerobic respiration on iron to drive ATP synthesis by the Mitchell hypothesis. It has been argued that at least two ferrous ions must be oxidized to provide sufficient redox potential energy to phosphorylate one ADP to ATP (Ingledew, Cox, & Halling, 1977; Tuovinen & Kelly, 1972).

Regardless of whether one, two, or even more ferrous ions must be oxidized to provide sufficient energy to generate each ATP, it is evident that the iron to molecular oxygen portion of the relevant electron transport chain must be relatively short, so as to not lose or waste energy with multiple electron transfer steps. Another consequence of this low energy yield is that there is likely to be an unusually high concentration of relevant electron transport components in any microorganism that conducts aerobic respiration on soluble iron for its predominant energy metabolism, because to do so requires a relatively high throughput of electrons. Classic 'divide and conquer' biochemical activities have been conducted for years on these acidophilic microorganisms in an effort to purify and characterize relevant individual electron transport proteins.

One unspoken, but common, goal of these studies is to eventually reassemble cell-free functional electron transport chains using the purified components. However, one who seeks to reassemble functional portions of respiratory electron transport chains using protein purified from obligate acidophiles is faced with hard choices regarding the best pH values to conduct any reconstruction or reassembly functional studies. This is particularly true in chemolithotrophs that oxidize soluble iron. It is generally accepted that the internal pH of these organisms is near neutrality. Soluble iron is readily autooxidized at higher pH values, where the product ferric ions are sparingly soluble. However, there is no evidence of abundant precipitated iron in the cytoplasms of any of these microorganisms. Consequently, the working hypothesis is that the soluble ferrous ion is oxidized at

the exterior of the plasma membrane, while the electrons thus obtained are passed to a terminal oxidase where the consumption of protons that accompanies the reduction of molecular oxygen occur at the expense of protons in the cytoplasm. In addition to the possibility of proton pumping concomitant with electron transport, this hypothesis provides for a vectoral consumption of protons in the cytoplasm that contributes to the proton gradient that is generally thought to drive the phosphorylation of ADP to generate ATP.

Any tertiary or quaternary polypeptides that span the plasma membrane are exposed to quite different pH environments, the acid pH (1.5−2.5 in typical laboratory cultures) outside the cell and the near neutral or slightly acid pH values (6−7) inside the cytoplasm of the cell. Portions of functional membrane proteins that are positioned on the acidic side of the intact plasma membrane may assume different conformations in cell-free preparations at neutral pH, while portions of membrane proteins that are positioned on the neutral side of the intact plasma membrane may be equally affected if they are exposed to the acidic pH normally encountered on the exterior of the intact plasma membrane. To circumvent this problem in cell-free studies using purified plasma membrane proteins, one could construct artificial spheroplasts such that the two sides of the artificial bilayer are exposed to vastly different pH values, but these are technically challenging experiments that are difficult to perform.

Alternatively, one could simply seek a new means to study respiratory electron transfer reactions *in situ* using intact microorganisms. The actual opportunity to study respiratory electron transport *in situ* has recently become much more plausible with the advent and accessibility of novel optical instruments known as integrating cavity absorption meters (ICAMs) that permit accurate absorbance measurements in turbid suspensions of live microorganisms (Blake et al., 2016; Blake & Griff, 2012; Li, Painter, Ban, & Blake, 2015). This chapter summarizes the observations to date on acidophilic chemolithotrophs using this new technology and speculates on the future applications/directions that this novel methodology may permit in *in situ* studies of intact microorganisms under physiological solution conditions.

2. Absorbance measurements in turbid suspensions

The redox-active prosthetic groups that are employed by respiratory electron transport proteins are invariably colored in the visible or near

UV-region. The ionic copper and iron-sulfur prosthetic groups have very small absorption coefficients, while the various heme groups that are employed by microorganisms are relatively highly colored with large absorption coefficients. All of these colored prosthetic groups tend to change color depending on whether they are undergoing oxidation or reduction. Regardless of the extent of these redox-dependent absorbance changes, each prosthetic group represents an intrinsic spectrophotometric probe whereby transient changes in the redox status of the molecule can be monitored with great sensitivity. In principle, one could monitor individual electron transfer reactions within an intact electron transport chain by simply monitoring the absorbance changes over time when an intact cell is exposed to an external reducing or oxidizing agent.

The principal problem in conducting absorbance spectroscopy of intact microorganisms in a conventional linear spectrophotometer is that intact bacteria are refractile bodies that scatter the measuring light. Three things can happen to the measuring light in a conventional linear spectrophotometer equipped with a standard 1-cm cuvette: it can be transmitted; it can be absorbed; or it can be scattered without absorption. In the latter case, the apparent attenuation of the measuring light reflects losses due to both true molecular absorption and light lost to scattering by the refractile intact microorganisms in the suspension (Merzlyak & Naqvi, 2000; Shibata, Benson, & Calvin, 1954). Initial efforts to conduct accurate absorbance measurements in turbid suspensions led Chance and colleagues over 50 years ago to develop and implement two new improvements on the standard single beam spectrophotometer in common use at that time. The first improvement was to divide the measuring light into two equal beams to interrogate duplicate turbid samples where absorbance changes were only occurring in one of the samples (Chance, 1951). Consequently, any contribution of turbidity to the apparent absorbance measurement could be negated by subtracting the value of the absorbance measurement in the turbid reference sample from that in the turbid, manipulated sample. The second improvement positioned a large-faced photomultiplier tube as close to the square sample chamber as was physically possible. The instrument operated with two beams of measuring light, one that scanned at multiple wavelengths and one that was fixed at a wavelength where minimal absorbance changes occurred to simply monitor the contribution to the scanned signal of scattering alone; this instrument was eventually marketed as the Aminco DW-2 spectrophotometer. While this was a great innovation at the time, more than half of the light that was scattered by the turbid sample still escaped the detector.

Subsequent alternative efforts to mitigate the contributions of light scattering to the acquisition of accurate absorbance measurements lead invariably to the notion that light scattering by turbid samples is not important if the actual measuring light is already as diffuse as it can get. Toward that end, novel integrating cavity absorption meters (ICAMs) have been described that are designed to quantify the total illumination that is introduced into a totally enclosed observation chamber. The premise is that a totally enclosed observation chamber can be constructed with a reflective/refractive inner surface such that the majority of the measuring light within the chamber is directed (eventually) to a single detector/photomultiplier tube. When there was a single source of light within the chamber, the ICAM was designed to quantify the number of photons derived from the point source of light (Kirk, 1997). When the sample was comprised of sea water taken from various locations around the globe, an ICAM with a relatively large volume was used to measure the slight color differences in the samples (Pope, Weidermann, & Fry, 2000). More importantly, when the sample contained suspension of living organisms/cells/tissues, an ICAM was used to conduct accurate absorbance measurements of the live samples that were free of scattering effects (Elterman, 1970; Fry, Kattawar, & Pope, 1992; Hodgkinson, Masiyano, & Tatam, 2009; Javorfi et al., 2006).

Fig. 1 shows a schematic diagram of a commercial ICAM that was constructed to enable accurate absorbance measurements of turbid suspensions of live microorganisms. Fig. 1A depicts a spherical cavity (a quartz round bottom flask) that is surrounded by a tightly packed proprietary white powder that serves to maximize the diffuse reflectance of light beyond the exterior surface of the spherical quartz flask. The neck of the round bottom flask, which provides ready access to the contents of the spherical cavity/observation cell, is filled in the illustration with a white polymer plug to minimize the loss of light from the chamber during recorded absorbance measurements. The apertures in the walls of the spherical cavity through which the measuring light enters and the transmitted/scattered light exits to the photomultiplier tube are positioned at a 90° angle such that the light has to undergo many reflections and cell transversals before it can be quantified using the photomultiplier tube. The moving slit depicted in Fig. 1A permits rapid spectral scans over a wavelength range of 100–300 nm, depending on the properties of the instrument's grating monochromator, at a rate as fast as 100 scans per second. The instrument illustrated in Fig. 1A is loosely based on those described by others (Elterman, 1970; Fry et al., 1992; Hodgkinson et al., 2009; Javorfi et al., 2006). To the extent that the particulate white

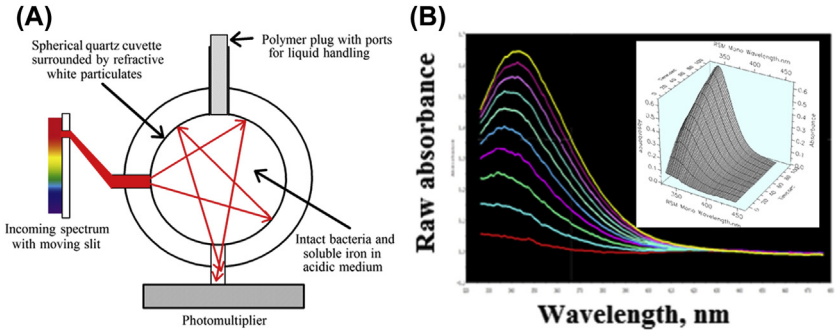

Fig. 1 Example of an integrating cavity absorption meter. (A) schematic cross section of an ICAM designed to permit accurate absorbance measurements in liquid media that scatter light. The moving slit creates spectral scans at rates of up to 100 scans per second. The light port to the photomultiplier is positioned at right angles to the light port through which the measuring light enters the spherical observation chamber. The spherical cuvette is surrounded by a refractive material that is designed to fully scatter the measuring light. The average effective path length of each photon is increased compared with traditional single-pass cuvettes, and the effects of light scattering are minimized or eliminated. (B) ten representative wavelength scans from 300 to 450 nm collected at a rate of 6.2 scans/second for 100 s after 2.1×10^9 cells of intact *L. ferriphilum* were introduced into 4.2 mL of 200 μM ferrous sulfate in sulfuric acid, pH 1.5, and 30 °C. *Inset*, all of the data collected in the scan in a 3-dimensional representation. These data were collected using a CLARiTY model 1000 ICAM marketed by On Line Instrument Systems, Inc., in Bogart, GA.

powder that surrounds the quartz chamber is able to maximize the diffuse reflectance of illumination within the chamber, an isotropic homogeneous field of light is created that minimizes the deleterious effects of light scattering when the cavity it filled with suspensions of live microorganisms. Another notable feature of this and other ICAMs is that the reflecting cavity acts as a multipass cuvette. That is, the effective path length of the observation chamber is considerably longer that the diameter of the cavity due to the multiple refractions at the cavity wall before each photon finally exits the chamber, a feature that provides much greater sensitivity.

An example of an absorbance measurement using this ICAM is shown in Fig. 1B. Fig. 1B shows the results that were obtained when 200 μM ferrous ions at pH 1.5 were mixed with 2.1×10^9 cells of intact *L. ferriphilum* at 30 °C. The *inset* of Fig. 1B shows a three-dimensional representation of the absorbance data collected at a rate of 6.2 averaged scans/s for 100 s over a wavelength range of 300–450 nm. Ten such averaged scans are shown in the main panel of Fig. 1B. The increase in absorbance with the

maximum wavelength at 355 nm represents the appearance of product ferric ions as the intact *L. ferriphilum* respired aerobically on soluble ferrous ions at that pH. In this example, the intact bacteria were present at a relatively low concentration to slow the rate of iron oxidation and to enable one to conduct steady-state kinetic analyses on the cell-catalyzed appearance of product ferric ions. Nonetheless, sufficient intact cells were suspended in this reaction mixture to prevent the acquisition of comparable kinetic absorbance data in a conventional linear spectrophotometer. Comparable absorbance measurements can be conducted at much higher cell concentrations with the goal of monitoring transient absorbance changes in the visible respiratory proteins in the intact cells themselves as they respire aerobically on soluble iron. Examples of both types of measurements are given below.

3. Steady state kinetic measurements

The dissimilatory oxidation or reduction of certain soluble metal ions is accompanied by corresponding changes in the absorbance properties of the metal ions. Soluble iron is one such metal ion (Turner & Miles, 1957). The data in Fig. 1B show the time- and bacterial cell-dependent increase in the absorbance at 355 nm as the soluble iron was oxidized from ferrous to ferric during the aerobic respiratory process. In this case, the increase in absorbance in the near UV provided a convenient spectrophotometric means to quantify the oxidation of soluble iron by intact cells. The primary absorbance spectra shown in Fig. 1B are presented as 'raw absorbance' because of prior reports that spectra obtained using integrated cavity absorption meters appear distorted when compared with corresponding spectra of the same materials obtained using a conventional linear spectrophotometer (Elterman, 1970; Fry et al., 1992; Hodgkinson et al., 2009; Javorfi et al., 2006). The *solid triangles* in Fig. 2 show the dependence of the raw absorbance values at 355 nm as a function of time when intact cells were mixed with ferrous iron at pH 1.5. The *dashed line* in Fig. 2 is a tangent to the curve created by the data, illustrating that the expected zero-order change in iron concentration was not observed with the primary raw data that were collected in this assay.

Unlike single path length spectrophotometers where the Beer-Lambert law dictates that the absorbance of a colored analyte at the appropriate wavelength should be directly proportional to the concentration of the analyte, the measuring light in an integrating sphere makes multiple random passes

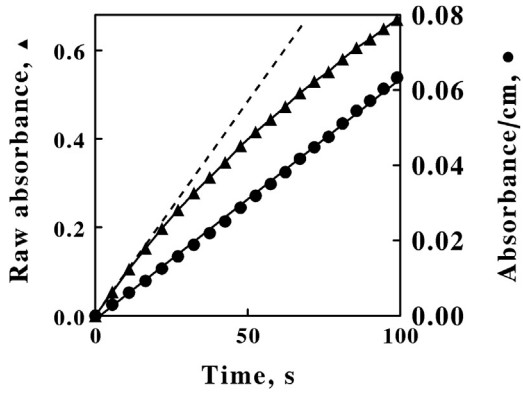

Fig. 2 Kinetic data at 355 nm as a function of time, extracted from the data set in Fig. 1B. The data represented by the solid triangles and the left ordinate show the raw absorbance values as collected in the ICAM. The data represented by the solid circles and the right ordinate show the corrected absorbance values obtained when the raw absorbance values were converted to equivalent absorbance values per cm using Eq. (4) in the text to adjust for mean path length differences.

with different path lengths that exacerbate the apparent nonlinearity with analyte concentration. While others have used semi-empirical methods to provide distortion-free spectra (Javorfi et al., 2006), Fry derived from first principles the following exact expression for fractional absorption in an integrating cavity absorption meter (Fry, Kattawar, Strycker, & Zhai, 2010; Fry et al., 1992):

$$1 - T = \frac{1 - \exp(-\alpha(\nu)LG)}{1 - \rho(1-h)\exp(-\alpha(\nu)LG)} \tag{3}$$

where T equals the observed transmittance in the integrating cavity absorption meter, $\alpha(\nu)$ equals the corresponding absorbance that would be observed in a spectrophotometer with a single path length of 1.0 cm, LG represents the mean geometric path length which for a sphere equals 2/3 of the sphere's diameter, ρ represents the reflectance at the walls of the cavity and is a number between 0 and 1, and h is the fraction of the cavity wall that is open for ports. Eq. (3) was rearranged to

$$\alpha(\nu) = -\ln\left[\frac{10^{-A}}{1 - \rho(1-h)(1-10^{-A})}\right] \Big/ LG \tag{4}$$

where A is the raw absorbance value observed in the ICAM and $\rho(1-h)$ was determined in separate experiments to be equal to 0.92 in the individual

instrument featured in Fig. 1 (data not shown). The *solid circles* in the *inset* of Fig. 2 were obtained when the raw absorbance values at 355 nm were converted to equivalent absorbance values per cm using Eq. (4). The converted absorbance values in Fig. 2 illustrate the enhanced sensitivity achieved in the ICAM where the mean path length of the measuring light is increased by multiple reflections around the interior of the cavity. As illustrated in Fig. 2, the soluble ferric ions that were produced in 100 s in the assay represented in Fig. 1B would have yielded an absorbance value of 0.063 in a standard 1-cm path length cuvette in a linear spectrophotometer, instead were observed to yield an apparent absorbance value of 0.64 in an ICAM that was equipped with a spherical cavity that had a total volume of 4.2 mL. The data conversion using Eq. (4) also eliminated the apparent distortion in the raw absorbance values wherein the absorbances at higher ferric concentrations appeared to be attenuated compared to the absorbances at lower iron concentrations. Thus those concentrations where greater absorption occurred received relatively higher values in the converted data than did those concentrations where lower absorption occurred. The data in Fig. 2 that were converted using Eq. (4) did obey the Beer-Lambert law with soluble ferric concentrations up to at least 100 s in the assay.

As illustrated in Fig. 1B, the formation of product ferric ions was evident as soon as intact cells of *L. ferriphilum* were introduced into an aerobic solution of ferrous ions at pH 1.5. The *inset* in Fig. 3 shows four representative time courses for the increases in absorbance at 355 nm that were obtained when 2.1×10^9 cells of *L. ferriphilum* were mixed with different concentrations of ferrous ions and monitored over time at 30 °C. Initial velocities of the changes in ferric concentration as a function of time were obtained from primary data such as those shown in the *inset* of Fig. 3, and the resulting secondary plot of initial velocity as a function of starting ferrous ion concentration is shown in the *main panel*. The parameters for the rectangular hyperbola drawn through the data points in Fig. 3 were derived from a nonlinear least squares fit of the Michaelis Menten equation to the initial velocity data. Values for Vmax and Km of 620 ± 20 nmol/min and 210 ± 30 μM, respectively, were obtained from the analysis.

The observations that aerobic respiration on soluble iron could be modeled using the Michaelis Menten equation were consistent with the minimal kinetic mechanism shown in Fig. 4. Briefly, the iron-dependent reduction of electron transport proteins in the bacterium is depicted as a relatively rapid reaction. The bacterium with its reduced cellular components is then shown as reacting with molecular oxygen to regenerate the oxidized

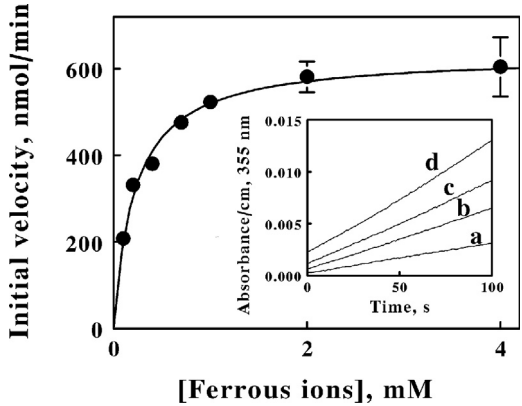

Fig. 3 Kinetic behavior of aerobic respiration on soluble iron by intact *L. ferriphilum* conforms to the Michaelis-Menten equation. Dependence of the initial velocity of ferric ion production on the concentration of ferrous ions when 2.1×10^9 cells of *L. ferriphilum* were included in 4.2 mL of sulfuric acid, pH 1.5, at 30 °C. Each *datum* represents the mean and standard deviation of at least five determinations. The parameters for the *curve* drawn through the data points were determined by a nonlinear regression analysis using the Michaelis Menten equation. *Inset*, representative examples of the increases in absorbance at 355 nm as a function of time due to the bacterially catalyzed production of ferric ions. The initial concentrations of ferrous ions were 0.1, 0.4, 1.0, and 4.0 mM in curves *a*—*d*, respectively.

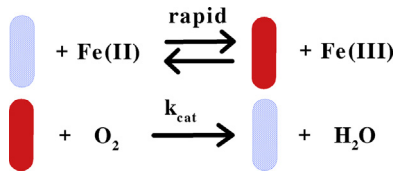

Fig. 4 Schematic representation of the kinetic mechanism for aerobic respiration on soluble iron as catalyzed by *L. ferriphilum*. The *cross-hatched* and *solid rods* represent bacteria that contain oxidized and iron-reduced electron transport proteins, respectively. *Reprinted from a prior publication (Blake, II, R.C., & Griff, M.N. (2012). In situ spectroscopy on intact Leptospirillum ferrooxidans reveals that reduced cytochrome 579 is an obligatory intermediate in the aerobic iron respiratory chain.* Frontiers in Microbiology, *3, 136).*

bacterium in a slower reaction that constitutes the rate-limiting catalytic step. The Michaelis complex in this model is portrayed as the electrochemically reduced microorganism.

Monod reported over seventy years ago that the rate of microbial growth appeared to be accurately modeled using the following rectangular

hyperbola when the concentration of a single growth substrate was limiting (Monod, 1949):

$$\mu = \frac{\mu_{max}[S]}{K_S + [S]} \quad (5)$$

where μ is the specific growth rate of the microorganism, μ_{max} is the maximum specific growth rate of the microorganism, [S] is the concentration of the limiting substrate for growth, and K_S is the value of [S] when $\mu/\mu_{max} = 0.5$. The Monod equation is generally applied to the growth rate of heterotrophic microorganisms when one organic substrate is clearly limiting. The limiting component in the growth rate of a strictly chemolithotrophic microorganism can easily be rationalized to be the biochemical energy required to fix carbon dioxide and/or atmospheric nitrogen. Thus the rate of growth and metabolism of both types of microorganisms can conform to the same type of mathematical model, whether it be the Monod model under conditions of limiting heterotrophic growth or the Michaelis Menten model under conditions of chemolithotrophic growth. Hyperbolic plots such as that shown for *L. ferriphilum* in Fig. 3 have also been reported for the cell-dependent oxidation of soluble iron as catalyzed by other chemolithotrophic microorganisms, including but not limited to, *L. ferrooxidans* (Blake & Griff, 2012), *At. ferrooxidans* (Li et al., 2015), *M. sedula*, *Sb. thermosulfidooxidans*, *Ap. aeolicum*, *Fp. acidiphilum*, and *Fm. acidiphilum* (the latter 5 hyperbolic plots are unpublished).

4. Cell-monitored turnover measurements

Once that one has the means to minimize the deleterious effects of light scattering on absorbance measurements, one is now free to examine transient absorbance changes in colored components within intact cells that are functioning under their normal physiological solution conditions. For a strict chemolithotroph like *L. ferriphilum* that respires aerobically on soluble iron, the relevant colored components within the intact cell are the redox-active chromophores that make up the aerobic respiratory chain. As an example, the spectra shown in Fig. 5A were obtained when air-oxidized cells of *L. ferriphilum* were exposed to 100 μM ferrous sulfate in sulfuric acid, pH 1.5. The six absorbance spectra shown in the figure were selected from a data set where 6.2 complete scans from 350 to 650 nm were collected every second for 250 s. The first spectrum was generated

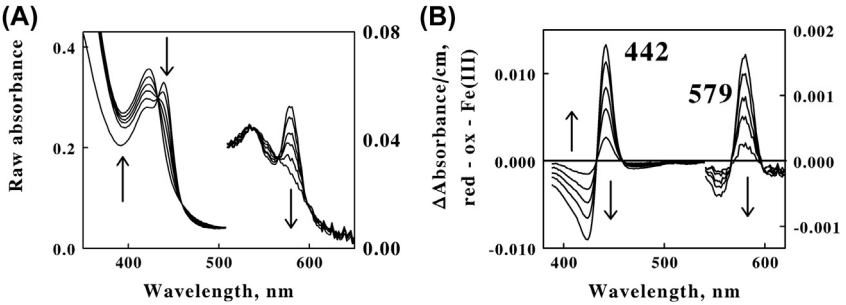

Fig. 5 Absorbance spectra obtained at different time points after 2.1 $\times$ 10^9 cells of intact *L. ferriphilum* were introduced into 4.2 mL of 100 μM ferrous sulfate in sulfuric acid, pH 1.5. (A) apparent absorbance spectra collected in the ICAM at six time points after mixing, ranging from 1.0 to 400s. Each *arrow* indicates whether the apparent absorbance at that wavelength increased or decreased with time. (B) difference spectra, representing the absolute spectrum of the iron-reduced *L. ferrooxidans* minus those obtained at selected time points following the initial reduction of the bacteria. The raw absorbances in panel A were converted to equivalent absorbance values per cm using Eq. (4) before the difference spectra were calculated. The absorbances at the longer wavelengths in both panels correspond to the more sensitive scales shown on the right ordinates.

within the operational dead time of mixing, roughly 0.5 s. It was characterized by an apparent cytochrome Soret peak that was split into two peaks with maxima at 420 and 442 nm. In addition, there was an absorbance peak in the typical cytochrome α,β region with a maximum absorbance at 579 nm. Subsequently, the peaks at 442 and 579 nm slowly decreased over a period of 150 s, while the oxidized peak at 420 nm gradually increased.

These spectral changes were consistent with the hypothesis that the cells respired aerobically on the soluble iron until the ferrous iron was completely oxidized. Thus the first spectrum represented cells that were partially or completely electrochemically reduced. Subsequent aerobic respiration under the conditions where the concentration of molecular oxygen exceeded that of the ferrous iron produced time-dependent changes in the observed spectra of whole cells until the limiting ferrous ions were completely oxidized. The stable spectrum that was obtained when the reduced iron was exhausted represented the spectrum of air-oxidized bacteria. The large time-dependent increases in absorbance below 400 nm were due to the increase in the ferric ion concentration as aerobic respiration proceeded.

Fig. 5B shows corrected difference spectra representing the absolute absorbance spectrum of the iron-reduced *L. ferriphilum* minus the spectra

obtained at various time points following the rapid reduction of the bacteria. The spectra of the corresponding concentrations of ferric iron were also subtracted from the differences. The two prominent peaks of the difference spectra occur at 442 and 579 nm. The observation of at least 4 relatively well-defined isosbestic points is extraordinary considering that the spectra were acquired in a highly turbid suspension of bacteria. An isosbestic point is a specific wavelength at which two or more absorbing species have the same molar absorptivity. The existence of those four well-defined isosbestic points suggests that there is only one principal iron-responsive cytochrome that is visible in the respiratory chain of *L. ferriphilum* while it is respiring aerobically on soluble iron.

Relating the transient, iron-dependent absorbance changes in *L. ferriphilum* to the appearance of oxidized soluble iron is no different in principle than relating the transient absorbance changes in the colored prosthetic groups employed by purified oxidoreductase enzymes as they catalyze their individual reactions, particularly when both systems catalyze reactions that obey the Michaelis Menten equation. Britton Chance was the first person to demonstrate over 75 years ago that Compound I, a 2-electron oxidized form of heme *b* that is transiently formed by horseradish peroxidase when the protein is exposed to hydrogen peroxide, fulfilled all of the mathematical and correlational requirements to represent the Michaelis complex in the horseradish peroxidase-catalyzed oxidation of malachite green by hydrogen peroxide (Chance, 1943). Chance's approach was later expanded to other oxidoreductases with colored prosthetic groups under the general title of 'enzyme-monitored turnover' measurements [Bright & Porter, 1975, and references therein]. In principle, the same approach can be applied to aerobic respiration on soluble iron as catalyzed by intact cells of *L. ferriphilum*.

The kinetic data shown in Fig. 6A were extracted from the data set that yielded the selected spectra shown in Fig. 5A. The change in absorbance at 355 nm, which represented predominantly the absorbance due to the time-dependent accumulation of ferric ions, increased in a roughly linear fashion until the limiting concentration of ferrous ions was completely depleted at around 110 s after the start of the bacterial-catalyzed reaction. The changes in absorbance at 442 nm, which represented the peak of the difference spectrum in the Soret region shown in Fig. 5B, slowly decreased over the time course of the reaction until about 90−100 s, when the absorbance then decreased rapidly back to the initial absorbance observed in the bacterium under air-oxidized conditions. It was evident that the cellular cytochrome

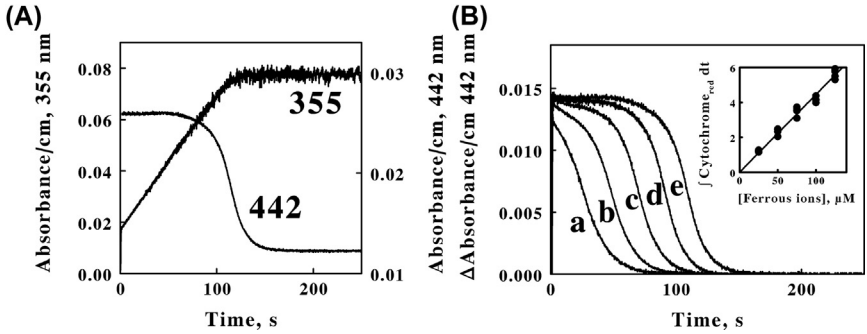

Fig. 6 The absorbance of the reduced cytochrome in intact *L. ferriphilum* correlates with the absorbance of ferric ions produced during aerobic respiration on soluble iron. (A) time courses of the absorbance changes at 355 and 442 nm obtained when 2.1×10^9 cells of *L. ferriphilum* were mixed with 100 μM ferrous sulfate in sulfuric acid, pH 1.5. (B) time courses of the differences in the absorbance changes at 442 nm obtained in the presence of different initial concentration of ferrous ions. Cells of *L. ferriphilum* (2.1×10^9) were introduced into sulfuric acid, pH 1.5, that contained 25, 50, 75, 100, and 125 μM ferrous sulfate in curves *a* through *e*, respectively; each curve represents the mean of four determinations. *Inset*, dependence of the areas swept out under the absorbance versus time curves on the initial concentration of ferrous ions.

returned to the oxidized state at about the same time that the product formation ceased.

If the cytochrome that exhibited the iron-reduced peaks at 442 and 579 nm in the difference spectra shown in Fig. 5B (hereafter referred to as cytochrome 579) is hypothesized to represent the 'Michaelis complex' of *L. ferriphilum* in Fig. 4, then the corresponding Michaelis Menten equation may be integrated to yield the following:

$$[\mathrm{Fe(II)}]_{\mathrm{Total}} = k_{\mathrm{cat}} \int [\text{reduced cytochrome } 579]\mathrm{d}t \qquad (6)$$

where the integral on the right side of the equality represents the total area swept out by the absorbance of the reduced cytochrome over time as illustrated by the 442 nm time course shown in Fig. 6A. The kinetic curves in Fig. 6B show the time courses of the absorbance changes at 442 nm that were obtained when constant concentrations of *L. ferriphilum* were mixed with different total concentrations of ferrous ions from 25 to 125 μM. Each trace was obtained in quadruplicate. The area under each trace was determined and plotted as a function of the starting ferrous concentration in the inset to Fig. 6B. The direct proportionality predicted by Eq. (6) is evident,

and the slope of the least-squares line shown in the *inset* of Fig. 6B yielded a value for k_{cat} of 37 s^{-1}.

This one example illustrates the intimate detail that may be extracted regarding the mechanism(s) of aerobic respiration when one can conduct accurate absorbance measurements on intact microorganisms. In principle, this cell-monitored turnover measurement can be conducted with any chemolithotrophic microorganism that can be described mathematically using the Michaelis Menten equation as it respires aerobically on soluble iron. The extension of these types of measurement to intact cells and other types of growth substrates is evident.

5. Measurements with different respiratory chains

5.1 Terminal oxidases in selected chemolithotrophs

The capacity to respire aerobically on soluble ferrous iron under strongly acidic conditions (pH < 3) is currently reported to be expressed in 42 species distributed among 19 genera in 6 phyla (Johnson, Kanao, & Hedrich, 2012). These six phyla are in turn distributed among Gram negative eubacteria, Gram positive eubacteria, and archaea (two phyla in each). Table 1 shows the results of tBLASTn searches for known types of terminal oxidases that are encoded in the genomes of 12 acidophilic, chemolithotrophic microorganisms, representing two genera chosen from each of the 6 phyla. The criteria for inclusion in Table 1 were 2-fold: a complete genome sequence for the microorganism had to be available and searchable; and spectrophotometric data had to be available that had been collected on the intact microorganism using an ICAM. The sequences of the terminal oxidases used to search the 12 genomes in Table 1 included 4 heme copper terminal oxidases (Sousa, Alves, Pereira-Leal, Teixeira, & Pereira, 2011) and two *bd*-type terminal oxidases (Borisov, Gennis, Hemp, & Verkhovsky, 2011; Giuffe et al., 2014). The data in Table 1 include a unique non-redundant protein accession number for each entry, a term that identifies the type of conserved protein domain that represents each terminal oxidase, and the precise gene locus tag where the nucleic acids that encode each protein may be found on the relevant genome.

Table 1 contains 54 entries: 19 *bd*-type terminal oxidases; and 35 heme copper terminal oxidases, which are divided into 3 cbb_3-type oxidases and 32 cytochrome *c*-type oxidases. The data in Table 1 yield a number of interesting observations. First, both genera in the Firmicutes phylum and one

Table 1 Terminal oxidases present in selected acidophiles that respire aerobically on soluble iron.

Microorganism	Protein accession number	Conserved protein domain present in the terminal oxidase	Locus Tag	Number of amino acids
Proteobacteria; Acidithiobacillia				
Acidithiobacillus ferrooxidans	WP_012536248.1	Cyt_c_Oxidase_I	AFE_RS02975	716
	WP_009561084.1	Cyt_c_Oxidase_I	AFE_RS14425	627
	WP_009567364.1	Cyt_bd_Oxidase_I	AFE_RS04470	544
Proteobacteria; Gammaproteobacteria				
Acidihalobacter ferrooxidans	WP_083699744.1	Cyt_c_Oxidase_I	BW247_RS01545	651
	WP_076835889.1	Cyt_c_Oxidase_I	BW247_RS03945	706
	WP_076836488.1	Cyt_c_Oxidase_I	BW247_RS06820	707
	WP_076836973.1	Ubiquinol_Oxidase_I	BW247_RS09695	682
	WP_076836130.1	Cyt_bd_Oxidase_I	BW247_RS04805	481
	WP_076836132.1	Cyt_bd_Oxidase_I	BW247_RS04815	481
	WP_076836135.1	Cyt_bd_Oxidase_I	BW247_RS04825	480
	WP_076837083.1	Cyt_bd_Oxidase_I	BW247_RS10385	550
	WP_076838585.1	Cyt_bd_Oxidase_I	BW247_RS12035	478
Nitrospirae				
Leptospirillum ferriphilum	WP_036082816.1	cbb3_Oxidase_I	LFTS_RS01635	460
	WP_014961552.1	cbb3_Oxidase_I	LFTS_RS04060	460
	WP_036081291.1	Cyt_bd_Oxidase_I	LFTS_RS09850	534
Leptospirillum ferrooxidans	WP_014448973.1	cbb3_Oxidase_I	LFE_RS03925	459
	WP_014449201.1	Cyt_bd_Oxidase_I	LFE_RS05190	528

Actinobacteria				
Acidimicrobium ferrooxidans	WP_015799102.1	Cyt_c_Oxidase_I	AFER_RS08835	649
	WP_015799214.1	Cyt_c_Oxidase_I	AFER_RS09415	563
	WP_015797981.1	Cyt_bd_Oxidase_I	AFER_RS02680	463
Ferrimicrobium acidiphilum	WP_035388637.1	Cyt_c_Oxidase_I	FEAC_RS03380	562
	WP_052566320.1	Cyt_c_Oxidase_I	FEAC_RS11735	649
Firmicutes; Bacilli				
Alicyclobacillus ferrooxydans	WP_054968196.1	Ubiquinol_Oxidase_I	AN477_RS05620	655
	WP_054969014.1	Cyt_c_Oxidase_I	AN477_RS10000	543
	WP_054970313.1	Ubiquinol_Oxidase_I	AN477_RS16735	657
	WP_054970316.1	Ubiquinol_Oxidase_I	AN477_RS16750	678
	WP_054970767.1	Cyt_c_Oxidase_I	AN477_RS19040	598
	WP_083486513.1	Cyt_c_Oxidase_I	AN477_RS19545	604
	WP_054971331.1	Ubiquinol_Oxidase_I	AN477_RS21905	654
	WP_054967273.1	Cyt_bd_Oxidase_I	AN477_RS00740	467
	WP_054968551.1	Cyt_bd_Oxidase_I	AN477_RS07550	461
Firmicutes; Clostridia				
Sulfobacillus thermosulfidooxidans	WP_020376323.1	Cyt_c_Oxidase_I	B8987_RS02260	647
	WP_084661870.1	Cyt_c_Oxidase_I	B8987_RS02445	627
	WP_028962690.1	Cyt_c_Oxidase_I	B8987_RS04255	623
	WP_081503227.1	Cyt_c_Oxidase_I	B8987_RS04780	618
	WP_084661190.1	Cyt_c_Oxidase_I	B8987_RS07830	648
	WP_084661417.1	Ubiquinol_Oxidase_I	B8987_RS09950	655
	WP_020376369.1	Cyt_bd_Oxidase_I	B8987_RS02240	479

(*Continued*)

Table 1 Terminal oxidases present in selected acidophiles that respire aerobically on soluble iron.—cont'd

Microorganism	Protein accession number	Conserved protein domain present in the terminal oxidase	Locus Tag	Number of amino acids
	WP_020376473.1	Cyt_bd_Oxidase_I	B8987_RS03025	470
	WP_084661348.1	Cyt_bd_Oxidase_I	B8987_RS09525	467
Euryarchaeota				
Acidiplasma aeolicum	WP_054964015.1	Cyt_c_Oxidase_I	SE19_RS02955	833
	WP_054963879.1	Cyt_bd_Oxidase_I	SE19_RS01265	485
	WP_054964292.1	Cyt_bd_Oxidase_I	SE19_RS06080	495
Ferroplasma acidiphilum	WP_081141379.1	Cyt_c_Oxidase_I	fad_RS00745	835
	WP_081141270.1	Cyt_bd_Oxidase_I	fad_RS00265	504
	WP_009886701.1	Cyt_bd_Oxidase_I	fad_RS07680	488
Crenarchaeota				
Metallosphaera sedula	WP_011921435.1	Cyt_c_Oxidase_I	MSED_RS01500	550
	WP_011921469.1	Cyt_c_Oxidase_I	MSED_RS01680	801
	WP_048060244.1	Cyt_c_Oxidase_I	MSED_RS02485	585
	WP_012020450.1	Cyt_c_Oxidase_I	MSED_RS02490	585
	WP_012020533.1	Cyt_c_Oxidase_I	MSED_RS02905	546
	WP_012021959.1	Cyt_c_Oxidase_I	MSED_RS10395	585
Sulfolobus metallicus	ABG91823.1	Cyt_c_Oxidase_I	Not applicable	595
	WP_083477006.1	Cyt_bd_oxidase_I	JMC9184_RS12275	499

genus in the Proteobacteria phylum each contain the genetic material to express up to 9 different terminal oxidases. What is the purpose of this extraordinary redundancy? The two Firmicutes in Table 1 are mixotrophs that are known to respire on selected organic compounds, soluble iron, reduced sulfur species, and selected metal-sulfide minerals like pyrite. Do these organisms have separate terminal oxidases for each type of growth substrate? Even so, why do they have the capacity to express up to 9 different terminal oxidases? Are there other growth substrates for these particular microorganisms that have not yet been identified?

Strictly chemolithotrophic microorganisms, whether they are the two species in the Nitrospirae phylum or the *Acidithiobacillus* genus in the Proteobacteria, only contain the genetic material to express 3 different terminal oxidases at the most. Similarly, those iron-oxidizing chemolithotrophs in the Actinobacteria and the Euryarchaeota phyla can each only express up to 3 different terminal oxidases. Finally the two genera in the Crenarchaeota phylum present an interesting contrast. The (as far as we know) strictly chemolithotrophic *S. metallicus* can express only 2 terminal oxidases, while the decidedly mixotrophic *M. sedula* has the capacity to express up to 6 different terminal oxidases.

Another interesting observation is that the cytochrome *bd* oxidases represent 35% of the terminal oxidases listed in Table 1. That is a higher percentage than the *bd*-type terminal oxidases enjoy in the general population of terminal oxidases that can be expressed in neutrophilic microorganisms. Cytochromes *bd* are electrogenic but they are generally not thought to pump protons (Borisov et al., 2011). Consequently, it is frequently suggested that these terminal oxidases may be preferentially expressed under acidophilic culture conditions where a steep proton gradient may already exist across the plasma membrane. Alternatively, others have suggested that cytochrome *bd* provides a higher resistance to classical terminal oxidase inhibitors like hydrogen sulfide (Giuffe et al., 2014). Any microorganism that respires on solid pyrite or other metal sulfide minerals is likely to be exposed to higher levels of hydrogen sulfide than those microorganisms that do not conduct such respiratory activities. Perhaps it is not surprising that *bd*-type oxidases may be more common in obligately acidophilic, chemolithotrophic microorganisms, like those featured in Table 1. Only two of the organisms shown in Table I, *Fm. acidiphilum* and *M. sedula*, do not appear to have the capacity to express a cytochrome *bd* terminal oxidase.

All of the cytochrome *c*-type terminal oxidases in the Table are annotated with reasonably conserved amino acids that comprise both a D- and

a K-channel for proton pumping activities concomitant with electron flow. These *c*-type terminal oxidases also share highly conserved amino acids for a single binuclear center, proton and water exit pathways, and a single low spin heme binding site. Six of the cytochromes in Table 1 are designated as ubiquinol oxidases because they also contain highly conserved amino acids for a quinol/ubiquinol binding site. Curiously, only the two species included in the Nitrospirae phylum appear to express exclusively cbb_3-type terminal oxidases and no cytochrome *c*-type oxidases. The cbb_3-type terminal oxidases are thought to only contain the K-channel for proton pumping activities (Melin et al., 2016).

Fig. 7 shows a rooted phylogenetic tree that was constructed using the sequences of the 19 *bd*-type cytochromes in Table 1, along with the sequences derived from 2 other *bd*-type oxidases obtained from neutrophilic microorganisms and a single heme copper oxidase from *M. sedula*. The

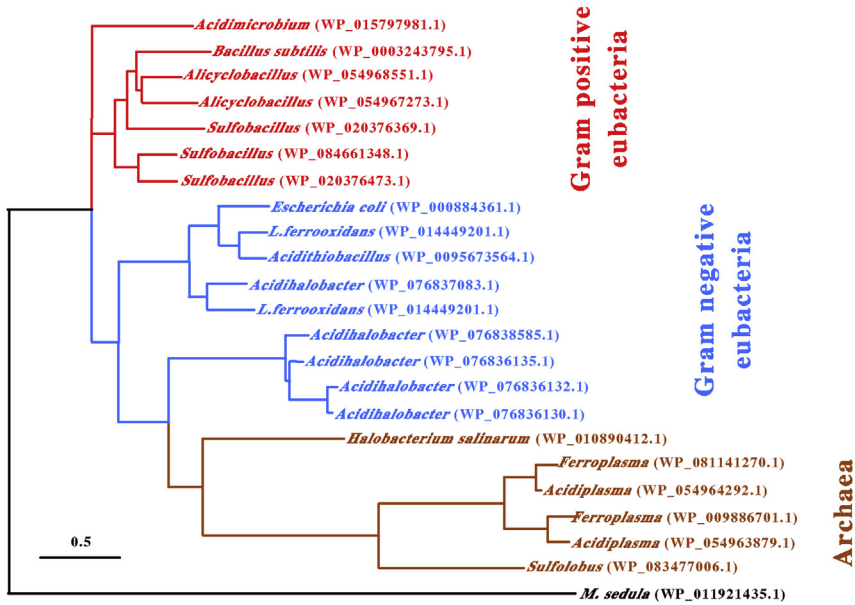

Fig. 7 Rooted phylogenetic tree based on 19 cytochrome *bd* amino acid sequences taken from the proteins represented by the accession numbers shown in Table 1. The outlying sequence (lowermost item shown in the figure) represents a heme copper oxidase present in the genome sequence of *M. sedula*. Two additional protein sequences present in the genomes of *Bacillus subtilis* and *Escherichia coli* were included in the tree to represent the cytochromes *bd* present in the genome sequences of neutrophilic Gram positive and Gram negative eubacteria, respectively. The tree was inferred using the maximum likelihood method with 1000 replicates.

bd-type oxidase sequences segregate into three groups that coincide with the inclusion of their respective microorganisms within either the Gram-negative eubacteria, the Gram-positive eubacteria, or the archaea. So, are the sequence similarities evident in the 3 groups identified in Fig. 7 simply a reflection of the overall phylogenetic proximities of the microorganisms, or do the different types of cell wall architectural features that are imposed by each type of microorganism play a role in selecting for common structural features among the integral membrane terminal oxidase proteins that are embedded in the different plasma membranes? Gram-negative eubacteria typically contain a relatively thin peptidoglycan layer adjacent to their plasma membrane. In addition to their thin peptidoglycan layer, the Gram negative bacteria also contain an outer membrane comprised of phospholipids and lipopolysaccharides (Beveridge, 1999). Gram positive eubacteria generally contain a single relatively thick layer of peptidoglycan that comprises a rigid cell wall around the outside of their plasma membrane. Most archaea possess a plasma membrane and an outer cell wall that is assembled from surface-layer proteins, which form a so-called S-layer (Sara & Sleytr, 2000). An S-layer is typically a rigid array of protein molecules that cover the outside of the archaeal cell like chain mail (Engelhardt & Peters, 1998); S-layers have been reported for the *Sulfolobus* and *Metallosphaera* genera (Veith et al., 2009). Notable exceptions to this general structural motif among archaea are that the three known species of *Ferroplasma* exhibit no S-layer and are simply bounded by a mere plasma membrane (Sleytr & Beveridge, 1999).

Fig. 8 shows a rooted phylogenetic tree that was constructed using the sequences of the 32 *c*-type terminal oxidases in Table 1, along with the sequences derived from 2 other *c*-type heme copper oxidases obtained from 2 neutrophilic Gram-negative microorganisms. Although it is generally true that the heme copper oxidase sequences derived from the Gram negative, the Gram positive, and the archaea still tend to segregate with each other on the tree, the groups of highly similar sequences also tend to be more interspersed than those observed for the *bd*-type cytochromes in Fig. 7.

5.2 Gram negative eubacteria

The Nitrospirae and the Proteobacteria are the two phyla of Gram-negative eubacteria that contain obligately acidophilic members that respire aerobically on soluble iron (Bonnefoy & Holmes, 2012). *Leptospirillum* is the only genus within the Nitrospirae that is known to contain acidophilic members that respire aerobically on soluble iron. Fig. 5B shows the reduced

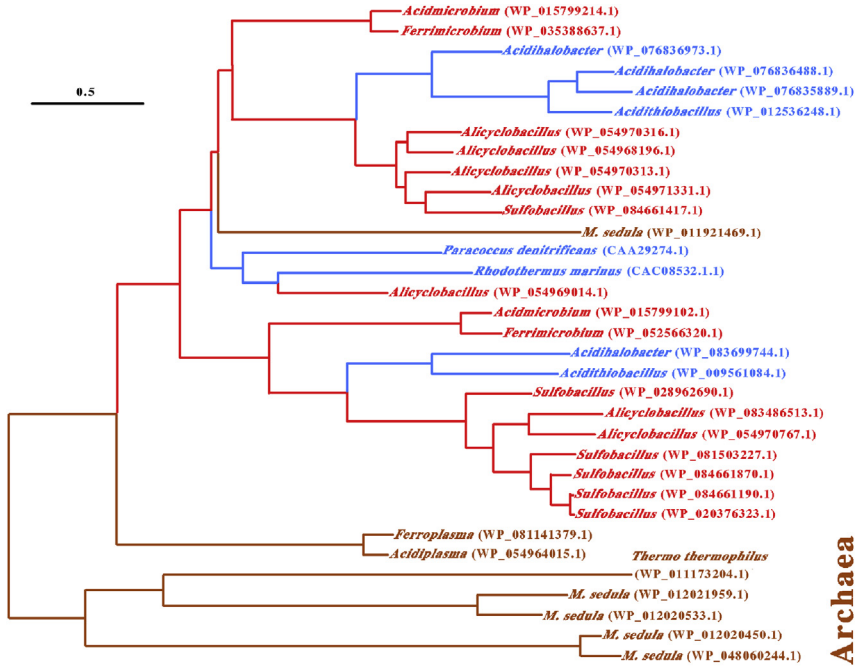

Fig. 8 Rooted phylogenetic tree based on 32 cytochrome *c*-type oxidase amino acid sequences taken from the proteins represented by the accession numbers shown in Table 1. The three outlying sequences included in the tree are the A1-, A2-. and B-type heme copper oxidases present in the genomes of *Paracoccus denitrificans*, *Rhodothermus marinus*, and *Thermo thermophilus*, respectively (Sousa et al., 2011). The tree was inferred using the maximum likelihood method with 1000 replicates.

minus oxidized difference spectrum that was obtained when intact *L. ferriphilum* was exposed to an excess of soluble ferrous ions in sulfuric acid at pH 1.5 using the ICAM. Identical experiments were conducted on intact *L. ferrooxidans* (Blake & Griff, 2012), and the results of both measurements are shown in Fig. 9. In both cases, the reduced peaks at 442 and 579 nm disappeared over a period of 5—7 min while the oxidized spectra (which would represent the baseline in these difference spectra) reappeared concomitantly (data summarized above for *L. ferriphilum*). These observations were consistent with the hypothesis that the cells respired aerobically on the soluble iron until the ferrous iron was completely oxidized by the excess of molecular oxygen that was dissolved in the solution. It is evident that in both cases, a cytochrome with a reduced absorbance peak at 579 nm was by far and away the principal absorbing species that underwent changes in its redox state during the respiratory reaction.

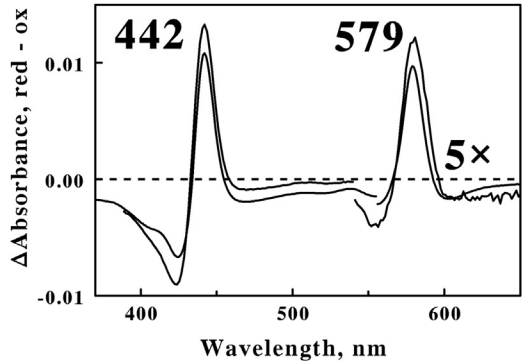

Fig. 9 Reduced minus oxidized difference spectra obtained when excess ferrous sulfate was mixed with intact cells of *L. ferriphilum* (higher absorbance) and *L. ferrooxidans* (lower absorbance), representing the Nitrospirae. The number of cells present in 8 mL of an ICAM were 1.3×10^9 and 1.9×10^9 for *L. ferriphilum* and *L. ferrooxidans*, respectively. The absorbance values in the α regions of both spectra were multiplied by 5 to aid in the clarity of presentation.

Prior reductionist studies on the identities and cellular locations of the respiratory chain components that are responsible for iron oxidation in the *Leptospirilli* reported that cell-free extracts derived from iron-grown *L. ferrooxidans* (Hart, Murrell, Poole, & Norris, 1991), *L. ferriphilum* (Ram et al., 2005), or a microbial biofilm community with a low diversity of microbes that was dominated by *Leptospirillum* group II bacteria (Singer et al., 2008) all contained readily discernible quantities of an acid-stable, acid-soluble cytochrome with an unusual absorbance maximum at 579 nm in the reduced state. Although the likely location of this cytochrome 579 was in the acidic periplasm, incomplete reduction of the protein was noted using 30 mM Fe(II) at pH 2.0. Another novel cytochrome with a unique reduced absorbance maximum at 572 nm was purified from the same biofilm communities (Jeans et al., 2008). Cytochrome 572, which was reported to be localized in the outer membrane, was readily and completely reduced by soluble Fe(II) at low pH. These observations led to the working hypothesis that cytochrome 572 was the initial iron oxidase in the outer membrane, while cytochrome 579 served to shuttle electrons from the outer membrane across the periplasm to a terminal oxidase in the plasma membrane.

We submit that there is no better way to establish the physiological relevance of a given biochemical reaction than to observe the progress of the reaction *in situ* as the intact microorganism functions under 'normal'

environmental conditions. Thus the ICAM measurements summarized herein support the hypothesis that cytochrome 579 plays a central role during aerobic respiration on iron in the relevant *Leptospirillum* species. Note that the transient difference spectra shown in Fig. 9 show no evidence of absorbance changes associated with a cytochrome with a reduced peak at 572 nm or a terminal oxidase that could either be a cbb_3-type heme copper oxidase or a *bd*-type cytochrome. Perhaps the other putative participants in the *Leptospirillum* electron transport chain are present in considerably lower concentrations than the cytochrome 579, or perhaps the kinetics of the individual electron transfer reactions within each chain are such that the rate-limiting step in either bacterium is oxidation of the cytochrome 579. This discussion illustrates a limitation in interpreting direct observations on electron transport reactions in intact microorganisms. Like any spectrophotometric measurement, only those species with significant absorbances or absorbance changes will be readily monitored.

Analogous ICAM measurements have been reported for two genera in the Proteobacteria phylum (Bonnefoy & Holmes, 2012). Proteobacteria that respire aerobically on soluble iron are distributed among at least 4 genera: *Acidithiobacillus, Acidiferrobacter, Acidihalobacter* and *Ferrovum*. The reduced minus oxidized difference spectrum obtained with intact *At. ferrooxidans* in the presence of soluble iron is shown in Fig. 10. The difference

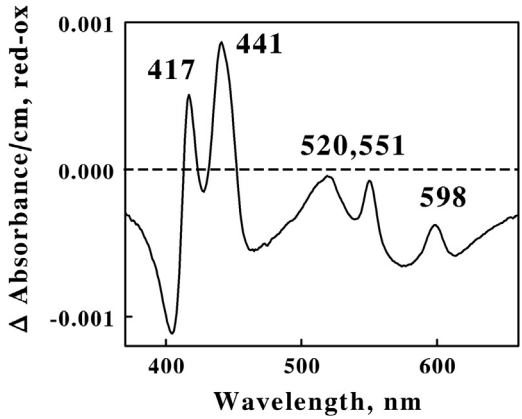

Fig. 10 Reduced minus oxidized difference spectrum obtained when excess ferrous sulfate was mixed with intact cells of *Acidithiobacillus ferrooxidans*, representing the Proteobacteria. The number of cells present in 8 mL of an ICAM were 4.6×10^9. The **bold numbers** identify the wavelengths where each peak exhibited its maximum value. *Adapted from a prior publication (Li, T. F., Painter, R. G., Ban, B., & Blake, II, R. C. (2015). The multicenter aerobic iron respiratory chain of* Acidithiobacillus ferrooxidans *functions as an ensemble with a single macroscopic rate constant.* Journal of Biological Chemistry, *290, 18293–18303).*

spectrum in Fig. 10 is relatively complex with up to 5 distinct peaks and valleys that may be seen to represent *c*-type cytochromes (peaks at 417, 520 and 551 nm), *a*-type cytochromes (peaks at 441 and 598 nm) and a blue copper protein known as rusticyanin (broad trough from 500 to 650 nm) (Li et al., 2015). The more extensive ICAM measurements that were conducted with intact *At. ferrooxidans* are discussed in more detail below in Section 6.

Fig. 11 shows the reduced minus oxidized difference spectrum that was observed when intact cells of air-oxidized *Ah. ferrooxidans* were exposed to excess ferrous ions at 35 °C and pH 1.5. This difference spectrum was different from that obtained with *At. ferrooxidans* in a number of ways. First, the difference spectrum in Fig. 11 exhibited no evidence of typical reduced cytochrome *c*-dependent absorbance changes around 417 or 550 nm. Second, the reduced peak at 565 nm in Fig. 11 was clearly in the spectral region normally attributed to the reduced peaks of *b*-type cytochromes, a feature that was absent in the spectrum obtained using intact *At. ferrooxidans*. Third, the first α peak encountered in the difference spectrum of *Ah .ferrooxidans* had a reduced peak at 608 nm, some 10 nm red-shifted from the equivalent peak seen in *At. ferrooxidans* at 598 nm. Finally, there was no evidence of a

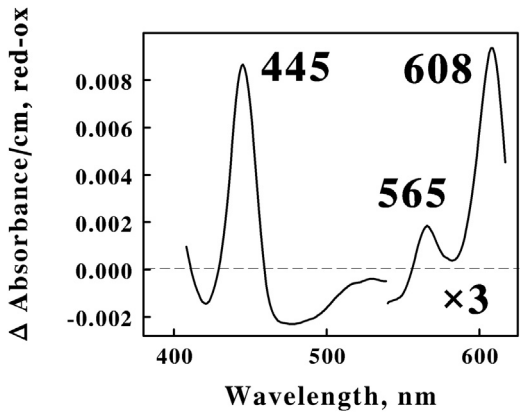

Fig. 11 Reduced minus oxidized difference spectra obtained when excess ferrous sulfate was mixed with intact cells of *Acidihalobacter ferrooxidans*, representing the Proteobacteria. The number of cells present in 8 mL of an ICAM were 2.7×10^9. The **bold numbers** identify the wavelengths where each peak exhibited its maximum value. The absorbance values in the α,β regions of the spectrum were multiplied by 3 to aid in the clarity of presentation. *Reprinted from a prior publication (Blake, II, R. C., Anthony, M. D., Bates, J. D., Hudson, T., Hunter, K. M., King, B. J., et al. (2016).* In situ *spectroscopy reveals that microorganisms in different phyla use different electron transfer biomolecules to respire aerobically on soluble iron.* Frontiers in Microbiology, 7, *1963).*

broad trough of negative absorbance in the spectrum in Fig. 11 that one could attribute to the iron-dependent reduction of a rusticyanin-like molecule.

Spectral properties similar to those shown in Fig. 11 have been reported for terminal oxidases expressed by two other Gram-negative eubacteria: *Thermus thermophilus*, a thermophile that grows at 70 °C (Zimmerman, Nitsche, Fee, Rusnak, & Munck, 1988); and *Rhodothermus marinus*, a thermohalophilic bacterium (Verissimo et al., 2007). The positions of the reduced α and β peaks varied between these two bacteria from 600 to 613 nm and from 577 to 562 nm, respectively. These absorbance properties were attributed to cytochrome *ba*3 terminal oxidases expressed by these two extremophilic eubacteria. A working hypothesis is that the absorbance properties shown in Fig. 11 represent a cytochrome *ba*3-type terminal oxidase that participates in the aerobic iron respiratory chain of the obligately halophilic and acidophilic *Ah. ferrooxidans*.

5.3 Gram positive eubacteria

The Firmicutes and the Actinobacteria are the two phyla of Gram-positive eubacteria that contain obligatory acidophilic members that respire aerobically on soluble iron (Bonnefoy & Holmes, 2012). These acidophilic bacteria are distributed among at least three genera in the Firmicutes: *Sulfobacillus, Alicyclobacillus*, and *Acidibacillus*. *Sulfobacillus* and *Alicyclobacillus* contain at least five and four separate species, respectively, that respire on iron.

Fig. 12 shows the reduced minus oxidized difference spectra that were observed when intact cells of *S. thermosulfidooxidans* and *Ali. ferrooxydans* were mixed with excess ferrous ions at pH 1.5 and 50 and 30 °C, respectively. Although the two difference spectra differed by several nanometers in both their reduced Soret and α peaks, the two spectra appeared to be sufficiently similar so as to represent the same type of heme prosthetic group embedded in slightly different protein environments. Because the positions of both reduced α peaks were greater than 600 nm, our hypothesis is that the spectra in Fig. 12 represent the respective terminal oxidases in the aerobic iron respiratory chains of these two Firmicutes.

Acidophilic bacteria that respire aerobically on soluble iron are distributed among at least five genera in the phylum Actinobacteria: *Acidimicrobium, Ferrimicrobium, Ferrithrix, Acidithrix*, and perhaps *Acidithiomicrobium*. Fig. 13 shows the reduced minus oxidized difference spectra that were observed when intact cells of *Am. ferrooxidans* and *Fm. acidiphilum* were mixed with excess ferrous ions at pH 1.5 and 45° and 32 °C, respectively.

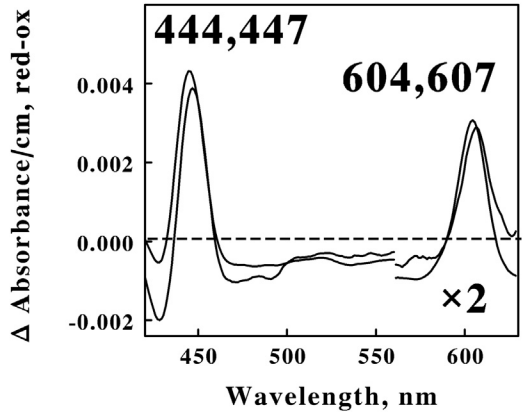

Fig. 12 Reduced minus oxidized difference spectra obtained when excess ferrous sulfate was mixed with intact cells of *Sulfobacillus thermosulfidooxidans* (lower wavelengths) and *Alicyclobacillus ferrooxydans* (higher wavelengths), representing the Firmicutes. The number of cells present in 8 mL of an ICAM were 6.8×10^{10} and 4.4×10^{10} for *Sb. thermosulfidooxidans* and *Ali. ferrooxydans*, respectively. The **bold numbers** identify the wavelengths where each peak exhibited its maximum value. The absorbance values in the α regions of both spectra were multiplied by 2 to aid in the clarity of presentation. *Reprinted from a prior publication (Blake, II, R. C., Anthony, M. D., Bates, J. D., Hudson, T., Hunter, K. M., King, B. J., et al. (2016).* In situ *spectroscopy reveals that microorganisms in different phyla use different electron transfer biomolecules to respire aerobically on soluble iron.* Frontiers in Microbiology, *7, 1963).*

As was the case with the two spectra shown in Fig. 12, the two difference spectra shown in Fig. 13 differed by only a few nanometers in both their reduced Soret and α peaks. Once again, the two spectra in Fig. 13 appeared to be sufficiently similar so as to represent the same type of heme prosthetic group embedded in slightly different protein environments. All four of the difference spectra shown in Figs. 12 and 13 are highly similar. The wavelengths of maximum absorbance of the reduced Sorets and α peaks in all four difference spectra support the hypothesis that each spectrum represents an *a*-type heme that is part of the terminal oxidase in its respective microorganism. The slight differences among the four spectra are presumed to be due to subtle structural differences among the respective globins that bind and function using the same *a*-type porphyrins. Thus the 4 Gram-positive eubacteria featured herein that respire aerobically on iron do so using basically the same principal redox-active prosthetic group in their respective terminal oxidases, regardless of the phylum or genus into which the bacterium is assigned on the basis of the sequence of its 16S ribosomal RNA.

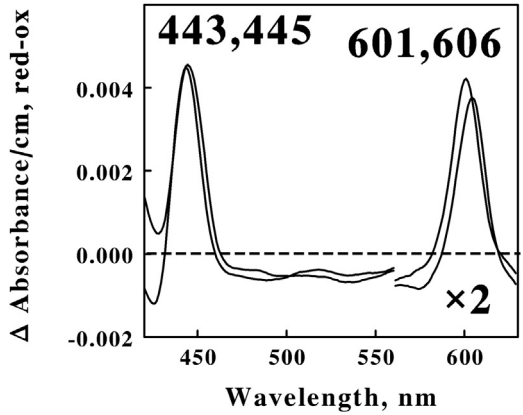

Fig. 13 Reduced minus oxidized difference spectra obtained when excess ferrous sulfate was mixed with intact cells of *Ferrimicrobium acidiphilum* (lower wavelengths) and *Acidimicrobium ferrooxidans* (higher wavelengths), representing the Actinobacteria. The number of cells present in 8 mL of an ICAM were 3.7×10^{10} and 3.1×10^{10} for *Fm. acidiphilum* and *Am. ferrooxidans*, respectively. The **bold numbers** identify the wavelengths where each peak exhibited its maximum value. The absorbance values in the α regions of both spectra were multiplied by 2 to aid in the clarity of presentation. *Reprinted from a prior publication (Blake, II, R. C., Anthony, M. D., Bates, J. D., Hudson, T., Hunter, K. M., King, B. J., et al. (2016).* In situ *spectroscopy reveals that microorganisms in different phyla use different electron transfer biomolecules to respire aerobically on soluble iron.* Frontiers in Microbiology, 7, *1963).*

5.4 Archaea

The Crenarchaeota and Euryarchaeota are the two phyla of Archaea that contain obligately acidiphilic members that respire aerobically on soluble iron (Bonnefoy & Holmes, 2012). These Archaea are distributed among two genera in the acidophilic Euryarchaeota: *Acidiplasma* and *Ferroplasma*. *Acidiplasma* and *Ferroplasma* contain at least two and three separate species, respectively, that respire aerobically on soluble iron. Fig. 14 shows the reduced minus oxidized difference spectra that were observed when intact cells of *Ap. aeolicum* and *Fp. acidiphilum* were mixed with excess ferrous ions at pH 1.5 and 40 and 35 °C, respectively. The absorbance of the reduced α peak observed with *Ap. aeolicum* had a maximum value at 583 nm, but there was also a discernible shoulder at longer wavelengths. The corresponding α region observed with iron-reduced *Fp. acidiphilum* exhibited two distinct peaks of absorbance, a more intense peak at 583 nm and a less intense peak at 594 nm. Others have reported the existence of an $a_{583}aa_3$-type of terminal oxidase in *S. tokodaii*, a member of

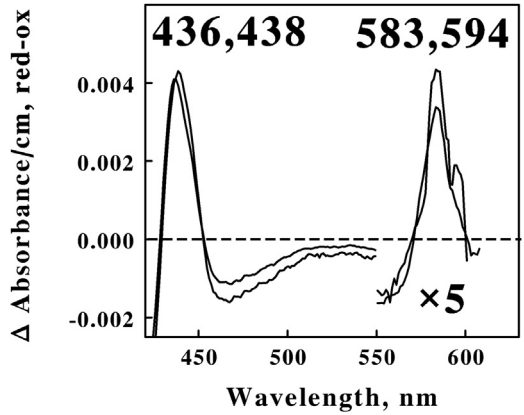

Fig. 14 Reduced minus oxidized difference spectra obtained when excess ferrous sulfate was mixed with intact cells of *Acidiplasma aeolicum* (lower wavelengths) and *Ferroplasma acidiphilum* (higher wavelengths), representing the Euryarchaeota. The number of cells present in 8 mL of an ICAM were 8.0×10^{10} and 9.5×10^{10} for *Ap. aeolicum* and *Fp. acidiphilum*, respectively. The **bold numbers** identify the wavelengths where each peak exhibited its maximum value. The absorbance values in the α,β regions of the spectrum were multiplied by 5 to aid in the clarity of presentation. *Reprinted from a prior publication (Blake, II, R. C., Anthony, M. D., Bates, J. D., Hudson, T., Hunter, K. M., King, B. J., et al. (2016).* In situ *spectroscopy reveals that microorganisms in different phyla use different electron transfer biomolecules to respire aerobically on soluble iron.* Frontiers in Microbiology, *7, 1963).*

the phylum Crenarchaeota (Iwasaki, Wakagi, Isogai, Iizuka, & Oshima, 1995; Schafer, 1996; Schafer, Purschkee, & Schmidt, 1996). The a_{583} component in the latter organism is also represented as heme A_S, an *a*-type heme with a formyl group on ring 1 and a hydroxyethylgeranylgeranyl side chain on ring 2 of the *a*-heme frame (Lubben & Morand, 1994). The accompanying aa_3 component of the terminal oxidase in *S. tokodaii* had a reduced α peak at 603 nm. Because the existence of a reduced α peak at 583 nm is rare, it seems reasonable to hypothesize that the terminal oxidases expressed by these two members of the Crenarchaeota represent a novel $a_{583}aa_3$-type of terminal oxidase where the aa_3 component differs slightly from that expressed in *S. tokodaii*.

Others have reported the purification and spectral characterization of two respiratory membrane protein complexes from cell-free extracts of *Fp. acidiphilum* (Castelle et al., 2015). One was a 850 kDa complex that contained an aa_3-type of cytochrome oxidase and a blue copper protein. This complex was tentatively identified as the principal iron oxidase used by the organism as it respired aerobically on soluble iron. The other was a

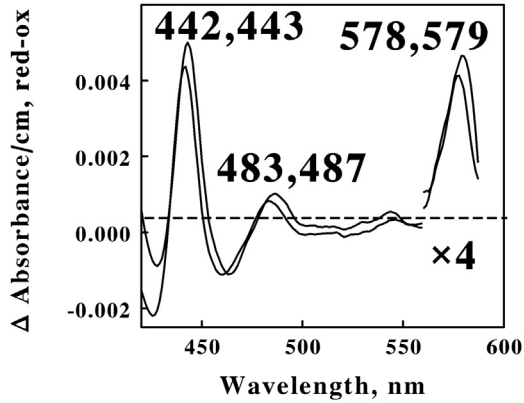

Fig. 15 Reduced minus oxidized difference spectra obtained when excess ferrous sulfate was mixed with intact cells of *Metallosphaera sedula* (lower wavelengths) and *Sulfolobus metallicus* (higher wavelengths), representing the Crenarchaeota. The number of cells present in 8 mL of an ICAM were 7.3×10^{10} and 1.2×10^{11} for *M. sedula* and *S. metallicus*, respectively. The **bold numbers** identify the wavelengths where each peak exhibited its maximum value. The absorbance values in the α regions of both spectra were multiplied by 4 to aid in the clarity of presentation. *Reprinted from a prior publication (Blake, II, R. C., Anthony, M. D., Bates, J. D., Hudson, T., Hunter, K. M., King, B. J., et al. (2016).* In situ *spectroscopy reveals that microorganisms in different phyla use different electron transfer biomolecules to respire aerobically on soluble iron.* Frontiers in Microbiology, *7, 1963).*

cytochrome *ba* complex that was proposed to conduct the 'uphill' electron flow from iron to generate NAD(P)H. The spectral properties of these two isolated protein preparations do not match those shown in Fig. 14.

Acidophilic bacteria that respire aerobically on soluble iron are distributed among four genera in the phylum Crenarchaeota: *Metallosphaera*, *Sulfolobus*, *Acidianus*, and *Sulfurococcus*. Fig. 15 shows the reduced minus oxidized difference spectra that were observed when intact cells derived from two genera of these Archaea were mixed with excess ferrous ions at pH 1.5 and 60 °C. Although the two difference spectra differed by several nanometers in all three peaks, the two spectra appeared to be sufficiently similar so as to represent the same prosthetic groups embedded in slightly different protein environments.

The first observation is that the reduced Soret and α peaks at around 422/423 and 578/579 nm, respectively, are remarkably similar to those shown above in Fig. 9 and reported for *L. ferrooxidans* (Blake & Griff, 2012; Singer et al., 2008) and *L. ferriphilum* (Li et al., 2015). Thus one can hypothesize that the same heme prosthetic group is expressed and utilized

for aerobic respiration on soluble iron by members of both the eubacterial Nitrospirae and the archaeal Crenarchaeota phyla. Interestingly, there is no evidence for genes in *M. sedula* or *S. metallicus* that encode a protein similar to the cytochrome 579 that is expressed in *L. ferrooxidans* or *L. ferriphilum*.

The second observation is that no spectral evidence was obtained for the participation of an $a_{583}aa_3$-type of terminal oxidase in either of these two representatives of Crenarchaeota, despite its existence in *S. tokodaii* (another member of the Crenarchaeota) and the participation of this latter terminal oxidase during respiration in the Euryarchaeota. The third observation was that a novel spectral species with a reduced peak at around 485 nm was observed when both Crenarchaeota were mixed with an excess of soluble ferrous ions. No evidence for a similar spectral peak was evident from the data reported for *Leptospirillum*. We know of no redox-active prosthetic group that exhibits a reduced peak in the vicinity of 485 nm. Perhaps this unexpected spectral intermediate represents a heretofore unknown and uncharacterized prosthetic group that is expressed and exploited by these Crenarchaeota as they respire aerobically on soluble iron.

The final observation is that the lone heme copper oxygen reductase encoded in the genome of *S. metallicus* differs sufficiently from the A-, B- and C-types of heme copper oxidases to be alternatively classified as a member of the F-family of heme copper oxidases (Hemp & Gennis, 2008). This protein was dubbed FoxA (Bathe & Norris, 2007). Interestingly, the genome of *M. sedula* also encodes two versions of FoxA: WP_012020450.1; and WP_048060244.1. Given the evident similarities between the two spectra shown in Fig. 15, it is tempting to hypothesize that both Crenarchaeota express and exploit a FoxA terminal oxidase to conduct aerobic respiration on soluble iron.

6. Detailed studies with *Acidithiobacillus ferrooxidans*

In situ ICAM measurements also have the potential to reveal new insights into the respiratory process even when the identities of the individual electron transport proteins are already known (Li et al., 2015). The respiratory chain of *At. ferrooxidans* has received the most attention among the obligate acidophiles that respire aerobically on iron. A generally accepted model for the iron respiratory chain of *At. ferrooxidans* comes from a combination of classic reductionist studies (Blake & Shute, 1994; Cavazza et al., 1996;

Giudici-Orticoni, Leroy, Nitschke, & Bruschi, 2000, 1999; Sugio, Ako, & Takeuchi, 2010; Yarzabal et al., 2002), bioinformatic analyses of genomic sequences (Appia-Ayme, Guiliani, Ratouchniak, & Bonnefoy, 1999; Bonnefoy & Holmes, 2012; Quatrini et al., 2009; Valdes et al., 2008), and proteomic and transcriptomic studies (Bouchal et al., 2006; Chi et al., 2007; Kucera et al., 2013; Quatrini et al., 2006; Yarzabal, Appia-Ayme, Ratouchniak, & Bonnefoy, 2004). The *rus* operon is hypothesized to encode all of the principal electron transport proteins that comprise the iron respiratory chain (Appia-Ayme et al., 1999). The primary oxidation of extracellular ferrous iron is thought to be accomplished by an outer-membrane cytochrome *c* (Blake & Shute, 1994; Yarzabal et al., 2002) that passes the electrons to rusticyanin, a type-I blue copper protein located in the periplasmic space of this Gram-negative organism (Cobley & Haddock, 1975; Cox & Boxer, 1978). These electrons are then transferred from the rusticyanin *via* a different periplasmic cytochrome *c* (Giudici-Orticoni, Guerlesquin, Bruschi, & Nitschke, 1999) to an aa_3-type terminal oxidase that spans the cytoplasmic membrane and transfers electrons to molecular oxygen (Kai, Yano, Tamegai, Fukumori, & Yamanaka, 1992; Sugio et al., 2010).

It is evident that all 3 types of electron transfer proteins hypothesized to participate in the aerobic iron respiratory chain of *At. ferrooxidans* are represented in the difference spectrum shown in Fig. 10. The spectra shown in Fig. 16 illustrate the approach taken to quantify the visible electron transport proteins in intact *At. ferrooxidans* that were transiently reduced by soluble iron. *Curve a* in Fig. 16 is a reduced minus oxidized difference spectrum for 13.4 nM cytochrome *a* that was calculated from spectra published using the electrophoretically homogeneous cytochrome oxidase purified from cell-free extracts of *At. ferrooxidans* (Sugio et al., 2010). *Curve c* in Fig. 16 is a difference spectrum for 20.6 nM cytochrome *c* that was calculated from published spectra of cytochrome *c* also purified from the same organism (Cavazza et al., 1996). Curve *b* in Fig. 16 is a difference spectrum for 311 nM rusticyanin that was calculated from the spectra of rusticyanin purified by several laboratories (Blake & Shute, 1987; Cox & Boxer, 1978). *Curve d* in Fig. 16 is the sum of *curves a*, *b*, and *c*. The data points overlaid on *curve d* in Fig. 16 represent the difference spectrum shown in Fig. 10. The close correspondence between the calculated and the observed spectra indicated that the ICAM measurements provided the means to quantify the concentration of each type of reduced protein in the intact cell.

When intact cells of *At. ferrooxidans* were exposed to soluble ferrous iron at concentrations in great excess to the limiting electron-accepting

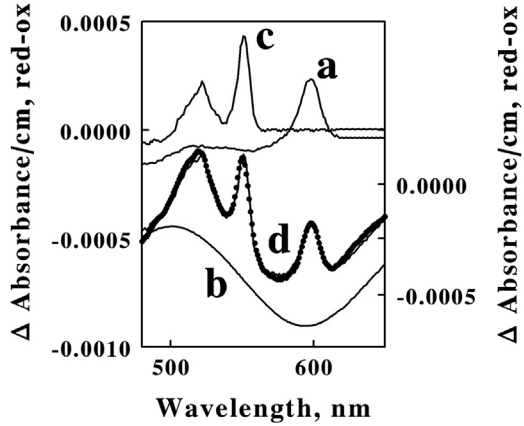

Fig. 16 Identification and quantification of principal electron transfer components that were reduced when intact *At. ferrooxidans* was exposed to soluble iron, representing the deconvolution into individual components of the difference spectrum obtained when *At. ferrooxidans* was reduced by 300 μM ferrous ions. *Curves a—c* are the reduced minus oxidized difference spectra for 13.5 nM cytochrome *a*, 311 nM rusticyanin, and 20.6 nM cytochrome *c*, respectively; *curve d* is the sum of *curves a—c*. The *data points* are those taken from Fig. 10. The rusticyanin difference spectrum was plotted using the *right ordinate* to aid in the clarity of presentation. *Adapted from a prior publication (Li, T. F., Painter, R. G., Ban, B., & Blake, II, R. C. (2015). The multicenter aerobic iron respiratory chain of* Acidithiobacillus ferrooxidans *functions as an ensemble with a single macroscopic rate constant.* Journal of Biological Chemistry*, 290, 18293—18303).*

capabilities of the molecular oxygen in the solution, ICAM measurements yielded a total rusticyanin concentration of 510 nM, which corresponds to 4.08 nmoles in the 8 mL volume of the observation cell of the ICAM (Li et al., 2015). At 0.31 μm^3 per cell, the total cellular volume of the 4.6×10^9 cells in the observation cell of the ICAM was thus 1.43×10^9 μm^3. We have been aware for many years that rusticyanin must be present at high concentrations in the periplasmic space of *At. ferrooxidans*; one early report stated that the periplasmic rusticyanin constituted as much as 5% of the total soluble protein expressed by the bacterium (Cobley & Haddock, 1975)! Values for the contribution of the periplasmic space to the total volume of a Gram-negative bacterium can vary from 10 to 20%, depending on whether one uses transmission electron microscopic measurements (Graham, Beveridge, & Nanninga, 1991) or compartment-specific radioactive tracers (Stock, Rauch, & Roseman, 1977), respectively, to estimate the fraction. Taking 15% as a compromise value, these data yield a periplasmic concentration for rusticyanin of 21.4 mM, or 350 mg/mL.

The latter value compares favorably with those of 330 mg/mL for hemoglobin in red blood cells (Doster & Longeville, 2007) and 300–400 mg/mL for macromolecules in the interior of *E. coli* (Zimmerman & Trach, 1991). The volume of a single rusticyanin molecule is approximately 20 nm^3, as determined using either the value of 0.73 cm^3/g for the average partial specific volume of a globular protein (Erickson, 2009), or the actual dimensions of the purified rusticyanin obtained from structural studies by X-ray crystallographic (Walter et al., 1996) or multidimensional NMR means (Botuyan, Toy-Palmer, Blake, Case, & Dyson, 1996). Consequently, the rusticyanin protein at 350 mg/mL occupies 4.6×10^{16} nm^3 or 21% of the total volume in the periplasmic space. Depending on how much of the 25 mg/mL of cytochrome *c* that was measured using the ICAM on the same sample (Li et al., 2015) is actually in the periplasm and how much is embedded in the outer membrane, one can estimate that this respiratory cytochrome could readily occupy another 2% of the periplasmic space. What emerges from these calculations is the image represented in Fig. 17, where the concentrations of respiratory proteins in the periplasm are orders of magnitude higher than any encountered in published *in vitro* functional studies. Studies conducted in dilute solutions have shown that (i) rusticyanin forms a complex with the periplasmic cytochrome *c* that lowers the standard reduction potential of the blue protein (Giudici-Orticoni et al., 1999) and (ii) the transfer of electrons

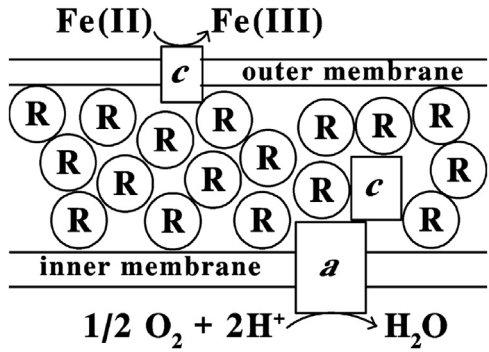

Fig. 17 Schematic representation of the principal electron transfer proteins in the periplasmic space of *At. ferrooxidans*, illustrating the macromolecular crowding and the relative quantities of the three types of components. **R**, ***a***, and ***c*** represent rusticyanin, cytochrome *a*, and cytochrome *c*, respectively. *Adapted from a prior publication (Li, T. F., Painter, R. G., Ban, B., & Blake, II, R. C. (2015). The multicenter aerobic iron respiratory chain of* Acidithiobacillus ferrooxidans *functions as an ensemble with a single macroscopic rate constant.* Journal of Biological Chemistry, *290, 18293–18303).*

from soluble Fe(II) to rusticyanin is catalyzed by the outer membrane cytochrome *c via* a transient encounter/Michaelis complex (Blake & Shute, 1994; Yarzabal et al., 2002). It is not a stretch of the imagination to hypothesize that additional interactions that serve to further influence their function and reactivity occur among the respiratory proteins at these high concentrations in the periplasm. An ancillary hypothesis is that these respiratory proteins have evolved to function as an ensemble in this crowded environment and that the crowded periplasmic space has a structure and order that we have not heretofore appreciated or characterized.

A test of this latter hypothesis was possible using the ICAM to monitor the time dependence of the changes in absorbance as the microorganism respired aerobically on soluble iron until the cells ran out of available molecular oxygen. Under solution conditions where the initial concentrations of ferrous ions were less than or equal to 400 μM, the absorbance spectrum of the cell suspension gradually changed from its partially reduced form back to its original air-oxidized form. Fig. 18A shows a series of rapid kinetic scans obtained when a cell suspension was mixed with 200 μM ferrous sulfate at pH 1.5. The first scan shows the spectrum of the partially reduced form of the cell suspension that was observed immediately, with the expected peaks at 520, 551, and 598 nm and a broad trough of lower absorbance over the entire region. Over the subsequent 200 s, the absorbance spectrum returned to that observed originally in the air-oxidized state.

Fig. 18B shows the spectral eigenvectors calculated from a multiwavelength global fit of the data set in Fig. 18A to a single exponential function of time, t:

$$\text{Absorbance} = (a - b)e^{-kt} + b \tag{7}$$

where *a* represents the spectrum of the reduced form of the suspension that was observed 0.5 s after mixing the cells with the soluble iron, *b* represents the spectrum of the final oxidized form of the suspension present at the end of the reaction, and k is the single pseudo-first order rate constant for all of the absorbance changes (DeSa & Matheson, 2004). The kinetic eigenvector obtained from the global fit analysis is represented by *curve b* in Fig. 18C. The smooth curve drawn through the data represents a single exponential function of time with a rate constant of $0.021 s^{-1}$. *Curve a* in Fig. 18C shows the actual absorbance changes at 580 nm that were extracted from the data set in Fig. 18A. The close correspondence between the actual absorbance at 580 nm and the computed eigenvector absorbance is evident. The increase

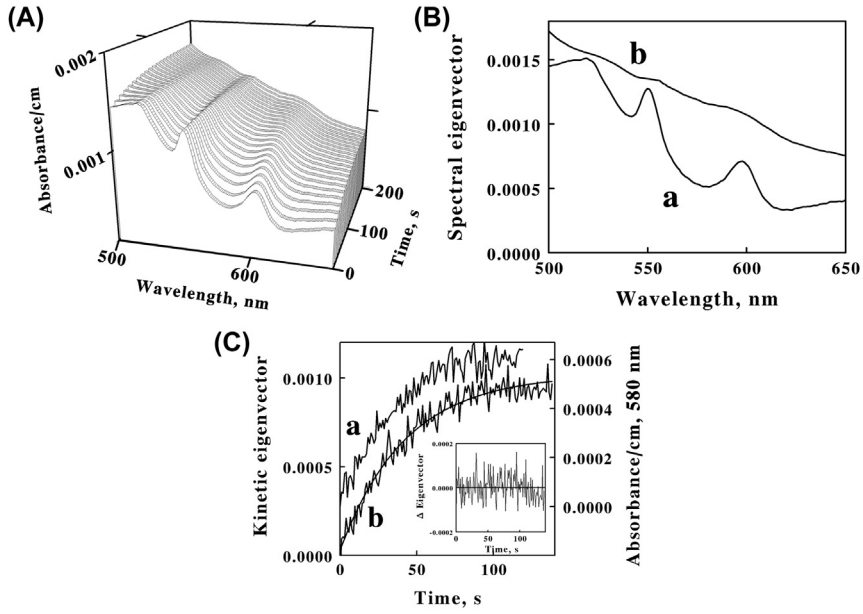

Fig. 18 Oxidation kinetics of iron-reduced *At. ferrooxidans*. (A) kinetic scans from 500 to 650 nm obtained when 4.6×10^9 cells of *At. ferrooxidans* were mixed with 200 μM ferrous sulfate, pH 1.5. The reaction was monitored at 30 °C in a dual-beam ICAM equipped with a rapid-scan module. Six scans were taken every second for 220 s; every 50th scan is presented. (B) spectral eigenvectors of the principal light-absorbing species present in the intact bacteria. Spectra were computed from a global fit of the data set represented in (A) to a single exponential function of time assuming the existence of two major species. Spectrum *a* was identical to that obtained 0.5 s after the cells were mixed with ferrous ions; spectrum *b* was identical to that obtained after the absorbance changes were complete. (C) comparison of the time-dependent oxidation of the bacteria monitored at 580 nm (*a*) with the kinetic eigenvector obtained from the global fit kinetic analysis (*b*). The *curve* drawn through the data in *b* represents a single exponential function of time with an apparent first-order rate constant of 0.021 s^{-1}. *Inset*, a residual plot of the differences between the kinetic eigenvector and the computed single exponential function of time. *Adapted from a prior publication (Li, T. F., Painter, R. G., Ban, B., & Blake, II, R. C. (2015). The multicenter aerobic iron respiratory chain of* Acidithiobacillus ferrooxidans *functions as an ensemble with a single macroscopic rate constant.* Journal of Biological Chemistry*, 290, 18293−18303).*

in absorbance at 580 nm is due predominantly to the oxidation of reduced rusticyanin. Favorable comparisons such as that shown in Fig. 18C were also obtained with data extracted at 550 and 598 nm, representing absorbance changes due primarily to cytochromes *c and a*, respectively (data not shown). It was evident that all of the absorbance changes in the data set shown in Fig. 18A can be adequately accommodated with a single exponential

function of time, despite the fact that three different electron transport proteins with quite different spectral and electrochemical properties all contributed to the overall absorbance changes.

Others have proposed that a respirasome comprised of a stable multi-protein complex bridges the periplasmic gap and provides a conduit to conduct electrons from the outer membrane to the terminal oxidase in the cytoplasmic membrane (Castelle et al., 2008). However, this hypothesis does not provide a role for the excess rusticyanin present in the periplasm, where the concentration of the small copper protein is 10-fold higher than those of the cytochromes *a and c* combined. Further, this hypothesis also does not present a rationale for the observations described herein, where the entire pool of available respiratory electrons reduces and oxidizes concomitantly as an ensemble with a single kinetic rate constant.

The data obtained *in situ* using the ICAM suggest an alternative hypothesis that the crowded, concentrated electron transport proteins in the periplasm of *At. ferrooxidans* constitutes a biological semi-conductor where the network of protein interactions functions effectively in the transport of electrons without a requirement for individual protein-protein binding specificities. The *in situ* electron transfer behavior summarized using *At. ferrooxidans* may be the rule, rather than the exception, in those chemolithotrophic bacteria that respire either aerobically or anaerobically with extracellular substrates (Bashir, Scanu, & Ubbink, 2011; Catarino & Turner, 2001; Paquete & Louro, 2014). We note that transient interactions among multi-heme cytochromes are widespread in the periplasmic spaces of *Shewanella* species that pass electrons to extracellular, insoluble iron oxides (Fonseca et al., 2013; Myers & Myers, 2001; Paquete, Saraiva, Calcada, & Louro, 2010; Shi et al., 2006). Similarly, respiratory electron transfer in the periplasm of *Paracoccus denitrificans* occurs *via* weak, ill-defined interactions among a pool of cytochromes, in contrast with the view that electron transport requires a defined linear series of molecular interactions (Meschi et al., 2011). Now that one has the capability to conduct accurate absorbance measurements of colored electron transfer proteins in suspensions of intact bacteria, it would be of interest to study the respiratomes of all of these microorganisms to investigate the generality of the *in situ* observations summarized herein.

7. Future applications of this method

If light scattering in turbid media is no longer an insurmountable experimental problem, it is evident that optical measurements other than

absorbance are possible in suspensions of intact cells. For example, one could conduct fluorescence measurements on whole cells. The measuring light in the absorbance measurement in the ICAM could serve as the excitation light in the corresponding fluorescence measurement. A suitable optical filter or a second monochromator could be placed at the portal where scattered light normally exits the spherical chamber. If this fluorescence emission light is very weak, the existing photomultiplier detector could be replaced with a suitable photon counter. One could anticipate that this might create a sensitive fluorimeter because of the isotropically homogeneous nature of the photons within the sample cavity. That is, all of the fluorophores within the cavity would be exposed to the exciting light, not just those that happened to be in the narrow path of the exciting beam of light in a one-pass cuvette in a conventional fluorimeter. Similarly, all of the emitted light would have the opportunity to be quantified in the single exit port of the spherical cavity, not just the photons that are emitted in the direction of the exit portal(s) set at right angles to the exciting light in a conventional linear fluorimeter. In the case of obligate chemolithotrophs, fluorescence measurements could perhaps be exploited to measure changes in the concentrations of NAD(P)H inside the intact cells as they respired on high reduction potential inorganic sources of electrons, like soluble iron. Curiosity regarding the mechanism(s) of the 'uphill' flow of electrons from soluble iron ($\sim$650 mV) to NAD(P)+ (~ -320 mV) has generated careful *in vitro* experimentation and hypotheses (Brasseur et al., 2004; Bruscella et al., 2007; Elbehti, Brasseur, & Lemesle-Meunier, 2000), but very little in the way of supporting *in situ* data, primarily because intracellular NAD(P)H concentrations are so technically difficult to quantify. The opportunity to measure NAD(P)H concentrations *in situ* by conducting fluorescence measurements in an ICAM would be a great boon to this work.

A second type of optical measurement that is possible in an ICAM could be quantification of molecular oxygen concentrations in cell suspensions as they respire aerobically on a suitable reduced substrate. There are a small number of luminescent organic molecules whose luminescence lifetimes and/or yield are a function of oxygen concentrations (Quaranta, Borisov, & Klimant, 2012).The observation chamber shown in Fig. 1A need not be limited to 2 portals of incoming and exiting light. The addition of two more light portals to the spherical observation chamber could permit one to use a new portal to (i) rapidly flash (excite) an exogenously-added probe whose luminescence lifetime or yield was sensitive to molecular oxygen and then to exploit the other new portal to (ii) monitor the properties of the

luminescence that emanates from the excited state of the probe. The advantage of using separate pairs of portals for absorbance and luminescence measurements is that the two measurements could be conducted in a rapidly alternating fashion on the same sample.

A third type of optical measurement that is possible in an ICAM could be the acquisition of a photochemical action spectrum. Carbon monoxide competitively inhibits the reactions of many heme proteins with molecular oxygen, including the heme copper oxidases in Table 1, by forming a heme-CO complex that can be dissociated with light absorption. For example, the ability of an ICAM to measure CO binding to a terminal oxidase of *Salmonella* Typhimurium was demonstrated in highly turbid samples of intact cells (Rana, McLean, Mann, & Poole, 2014). This CO-binding phenomenon results in an inhibition of oxygen consumption by the terminal oxidase in the dark, an inhibition that is relieved by light. This light induced relief of respiratory inhibition is dependent on the absorption coefficient of the heme-CO complex at each wavelength. Thus the relief of inhibition defines the absorption coefficient of the heme-CO complex in the terminal oxidase of the respiratory reaction under consideration (Rosenthal & Cooper, 1967; Wilson, 2004, and references therein). This was the method that revealed that the cytochrome P-450 system in the mammalian liver was the catalytic agent that was primarily responsible for the hydroxylation and oxidative metabolism of foreign organic compounds in the blood (Cooper, Levin, Narasimhulu, Rosenthal, & Estabrook, 1965). This could be a very useful method to help identify the actual terminal oxidase(s) in those microorganisms featured above, like *Leptospirillum* and perhaps the Crenarchaeota, where the redox-active chromophores identified in the existing ICAM absorbance measurements might not be the terminal oxidases.

A fourth type of measurement could involve the insertion of ion-selective electrodes into the reaction observation chamber illustrated in Fig. 1A. If light scattering is no longer a significant problem in optical measurements, then the insertion of one or more ion selective microelectrodes into the observation chamber should not disturb the acquisition of accurate absorbance, fluorescence, or luminescence lifetime measurements. Such a setup might be particularly useful when studying aerobic respiration on reduced sulfur species, when ion selective microelectrodes for the spectroscopically invisible thiosulfate, tetrathionate, and sulfide are readily available. In principle, one could measure the concentration of a reduced sulfur species, the absorbance of an intact microorganism, and the concentration of molecular oxygen concomitantly in the same reaction mixture.

Although we have presented these instrumental scenarios as hypothetical, the hardware and software necessary to bring all of these measurement capabilities to fruition are essentially available for beta testing at this time. Last, but not least, the insertions of working, counter, and reference microelectrodes into the observation chamber of an ICAM could permit one to conduct spectroelectrochemical measurements on intact cells under physiological solution conditions. Preliminary spectroelectrochemical measurements in our laboratory have been very promising.

Acknowledgments

RCB gratefully acknowledges the financial support provided by the National Science Foundation Grant 1830866.

References

Alexander, B., Leach, S., & Ingledew, W. J. (1987). The relationship between chemiosmotic parameters and sensitivity to anions and organic acids in the acidophile *Thiobacillus ferrooxidans*. *Journal of General Microbiology, 133*, 1171–1179.

Appia-Ayme, C., Guiliani, N., Ratouchniak, J., & Bonnefoy, V. (1999). Characterization of an operon encoding two *c*-type cytochromes, an aa_3-type cytochrome oxidase, and rusticyanin in *Thiobacillus ferrooxidans* ATCC 33020. *Applied and Environmental Microbiology, 65*, 4781–4784.

Bashir, Q., Scanu, S., & Ubbink. (2011). Dynamics in electron transfer protein complexes. *FEBS Journal, 278*, 1391–1400.

Bathe, S., & Norris, P. R. (2007). Ferrous iron- and sulfur-induced genes in *Sulfolobus metallicus*. *Applied and Environmental Microbiology, 73*, 2491–2497.

Beveridge, T. J. (1999). Structures of Gram-negative cell walls and their derived membrane vesicles. *Journal of Bacteriology, 181*, 4725–4733.

Blake, R. C., II, Anthony, M. D., Bates, J. D., Hudson, T., Hunter, K. M., King, B. J., et al. (2016). *In situ* spectroscopy reveals that microorganisms in different phyla use different electron transfer biomolecules to respire aerobically on soluble iron. *Frontiers in Microbiology, 7*, 1963.

Blake, R. C., II, & Griff, M. N. (2012). In situ spectroscopy on intact Leptospirillum ferrooxidans reveals that reduced cytochrome 579 is an obligatory intermediate in the aerobic iron respiratory chain. *Frontiers in Microbiology, 3*, 136.

Blake, R. C., II, & Shute, E. A. (1987). Respiratory enzymes of *Thiobacillus ferrooxidans*: A kinetic study of electron transfer between iron and rusticyanin in sulfate media. *Journal of Biological Chemistry, 262*, 14983–14989.

Blake, R. C., II, & Shute, E. A. (1994). Respiratory enzymes of *Thiobacillus ferrooxidans*: Kinetic properties of an acid-stable iron:rusticyanin oxidoreductase. *Biochemistry, 33*, 9220–9228.

Bonnefoy, V., & Holmes, D. S. (2012). Genomic insights into microbial iron oxidation and iron uptake strategies in extremely acidic environments. *Environmental Microbiology, 14*, 1597–1611.

Borisov, V. B., Gennis, R. B., Hemp, J., & Verkhovsky, M. I. (2011). The cytochrome *bd* respiratory oxygen reductases. *Biochimica et Biophysica Acta, 1807*, 1398–1413.

Botuyan, M. V., Toy-Palmer, A., Blake, R. C., II, Case, D. A., & Dyson, H. J. (1996). NMR solution structure of Cu(I) rusticyanin from *Thiobacillus ferrooxidans*: Structural basis for the extreme acid stability and redox potential. *Journal of Molecular Biology, 263*, 752–767.

Bouchal, P., Zdrahal, Z., Helanova, S., Janiczek, O., Hallberg, K. B., & Mandl, M. (2006). Proteomic and bioinformatics analyses of iron- and sulfur-oxidizing *Acidithiobacillus ferrooxidans* using immobilized pH gradients and mass spectrometry. *Proteomics, 6*, 4278–4285.

Brasseur, G., Levican, G., Bonnefoy, V., Holmes, D., Jedlicki, E., & Lemesle-Meunier, D. (2004). Apparent redundancy of electron transfer pathways via b*c1* complexes and terminal oxidases in the extremophilic chemolithoautotrophic *Acidithiobacillus ferrooxidans*. *Biochimica et Biophysica Acta, 1656*, 114–126.

Bright, H. J., & Porter, D. J. T. (1975). Flavoprotein oxidases. In P. D. Boyer (Ed.), *The enzymes XII: Oxidation reduction part B* (3rd ed., pp. 421–505). New York, NY: Academic Press.

Bruscella, P., Appia-Ayme, C., Levica, G., Ratouchniak, J., Jedlicki, E., Holmes, D. S., et al. (2007). Differential expression of two b*c1* complexes in the strict acidophilic chemolithoautotrophic bacterium *Acidithiobacillus ferrooxidans* suggests a model for their respective roles in iron or sulfur oxidation. *Microbiology, 153*, 102–110.

Castelle, C., Guiral, M., Malarte, G., Ledgham, F., Leroy, G., Brugna, M., et al. (2008). A new iron-oxidizing/O_2-reducing supercomplex spanning both inner and outer membranes, isolated from the extreme acidophile *Acidithiobacillus ferrooxidans*. *Journal of Biological Chemistry, 283*, 25803–25811.

Castelle, C. J., Roger, M., Bauzan, M., Brugna, M., Lignon, S., Nimtz, M., et al. (2015). The aerobic respiratory chain of the acidophilic archaeon *Ferroplasma acidiphilum*: A membrane-bound complex oxidizing ferrous iron. *Biochimica et Biophysica Acta, 1847*, 717–728.

Catarino, T., & Turner, D. L. (2001). Thermodynamic control of electron transfer rates in multicenter redox proteins. *ChemBioChem, 2*, 416–424.

Cavazza, C., Guidici-Orticoni, M. T., Nitschke, W., Appia, C., Bonnefoy, V., & Bruschi, M. (1996). Characterization of a soluble cytochrome c_4 isolated from *Thiobacillus ferrooxidans*. *European Journal of Biochemistry, 242*, 308–314.

Chance, B. (1943). The kinetics of the enzyme-substrate compound of peroxidase. *Journal of Biological Chemistry, 151*, 553–577.

Chance, B. (1951). Rapid and sensitive spectrophotometry. III. A double beam apparatus. *Review of Scientific Instruments, 22*, 634–638.

Chi, A., Valenzuela, L., Beard, S., Mackey, A. J., Shabanowitz, J., Hunt, D. F., et al. (2007). Periplasmic proteins of the extremophile *Acidithiobacillus ferrooxidans*: A high throughput proteomics analysis. *Molecular & Cellular Proteomics, 6*, 2239–2251.

Cobley, J. G., & Haddock, B. A. (1975). The respiratory chain of *Thiobacillus ferrooxidans*: The reduction of cytochromes by Fe^{2+} and the preliminary characterization of rusticyanin a novel "blue" copper protein. *FEBS Letters, 60*, 29–33.

Cooper, D. Y., Levin, S., Narasimhulu, S., Rosenthal, O., & Estabrook, R. W. (1965). Photochemical action spectrum of the terminal oxidase of mixed function oxidase systems. *Science, 147*, 400–402.

Cox, J. C., & Boxer, D. H. (1978). The purification and some properties of rusticyanin, a blue copper protein involved in iron(II) oxidation from *Thiobacillus ferrooxidans*. *Biochemical Journal, 174*, 497–502.

DeSa, R. J., & Matheson, I. B. C. (2004). A practical approach to interpretation of singular value decomposition results. *Methods in Enzymology, 384*, 1–8.

Doster, W., & Longeville, S. (2007). Microscopic diffusion and hydrodynamic interactions of hemoglobin in red blood cells. *Biophysical Journal, 93*, 1360–1368.

Elbehti, A., Brasseur, G., & Lemesle-Meunier, D. (2000). First evidence for existence of an uphill electron transfer through the b*c1* and NADH-Q oxidoreductase complexes of the acidophilic obligate chemolithotrophic ferrous ion-oxidizing bacterium *Thiobacillus ferrooxidans*. *Journal of Bacteriology, 182*, 3602–3606.

Elterman, P. (1970). Integrating cavity spectroscopy. *Applied Optics, 9*, 2140–2142.
Engelhardt, H., & Peters, J. (1998). Structural research on surface layers: A focus on stability, surface layer homology domains, and surface layer-cell wall interactions. *Journal of Structural Biology, 124*, 276–302.
Erickson, H. P. (2009). Size and shape of protein molecules at the nanometer level determined by sedimentation, gel filtration, and electron microscopy. *Biological Procedures Online, 11*, 32–51.
Fonseca, B. M., Paquete, C. M., Neto, S. E., Pacheco, I., Soares, C. M., & Louro, R. O. (2013). Mind the gap: Cytochrome interactions reveal electron pathways across the periplasm of *Shewanella oneidensis* MR-1. *Biochemical Journal, 449*, 101–108.
Fry, E. S., Kattawar, G. W., & Pope, R. M. (1992). Integrating cavity absorption meter. *Applied Optics, 31*, 2055–2065.
Fry, E. S., Kattawar, G. W., Strycker, B. D., & Zhai, P. W. (2010). Equivalent path lengths in an integrating cavity: Comment. *Applied Optics, 49*, 575–577.
Ghosh, W., & Dam, B. (2009). Biochemistry and molecular biology of lithotrophic sulfur oxidation by taxonomically and ecologically diverse bacteria and archaea. *FEMS Microbiology Reviews, 33*, 999–1043.
Giudici-Orticoni, M. T., Guerlesquin, F., Bruschi, M., & Nitschke, W. (1999). Interaction-induced redox switch in the electron transfer complex rusticyanin-cytochrome c_4. *Journal of Biological Chemistry, 274*, 30365–30369.
Giudici-Orticoni, M. T., Leroy, G., Nitschke, W., & Bruschi, M. (2000). Characterization of a new diheme c_4-type cytochrome isolated from *Thiobacillus ferrooxidans*. *Biochemistry, 39*, 7205–7211.
Giuffre, A., Borisov, V. B., Arese, M., Sarti, P., & Forte, E. (2014). Cytochrome *bd* oxidase and bacterial tolerance to oxidative and nitrosative stress. *Biochimica et Biophysica Acta, 1837*, 1178–1187.
Grabarczyk, D. B., & Berks, B. C. (2017). Intermediates in the Sox sulfur oxidation pathway are bound to a sulfane conjugate of the carrier protein SoxYZ. *PLoS One, 12*, e0173395.
Graham, L. L., Beveridge, T. J., & Nanninga, N. (1991). Periplasmic space and the concept of the periplasm. *Trends in Biochemical Sciences, 16*, 328–329.
Harrison, A. P., Jr. (1984). The acidiphilic Thiobacilli and other acidophilic bacteria that share their habitat. *Annual Reviews of Microbiology, 38*, 265–292.
Hart, A. J., Murrell, J. C., Poole, R. K., & Norris, P. R. (1991). An acid-stable cytochrome in iron-oxidizing *Leptospirillum ferrooxidans*. *FEMS Microbiology Letters, 81*, 89–94.
Hemp, J., & Gennis, R. B. (2008). Diversity of the heme–copper superfamily in archaea: Insights from genomics and structural modeling. In G. Schäfer, & H. S. Penefsky (Eds.), *Bioenergetics. Results and problems in cell differentiation* (Vol. 45, pp. 1–31). Berlin, Heidelberg: Springer.
Hodgkinson, J., Masiyano, D., & Tatam, R. P. (2009). Using integrating spheres as absorption cells: Path-length distribution and application of Beer's law. *Applied Optics, 48*, 5748–5758.
Ingledew, W. J. (1982). *Thiobacillus ferrooxidans*: The bioenergetics of an acidophilic chemolithotroph. *Biochimica et Biophysica Acta, 683*, 89–117.
Ingledew, W. J., & Cobley, J. C. (1980). A potentiometric and kinetic study on the respiratory chain of ferrous-grown *Thiobacillus ferrooxidans*. *Biochimica et Biophysica Acta, 590*, 141–158.
Ingledew, W. J., Cox, J. C., & Halling, P. J. (1977). A proposed mechanism for energy conservation during Fe^{2+} oxidation by *Thiobacillus ferrooxidans:* Chemiosmotic coupling to net H^+ influx. *FEMS Microbiology Letters, 2*, 193–197.
Iwasaki, T., Wakagi, T., Isogai, Y., Iizuka, T., & Oshima, T. (1995). Resolution of the aerobic respiratory system of the thermoacidophilic archaeon, *Sulfolobus* sp. *strain* 7. *Journal of Biological Chemistry, 270*, 30893–30901.

Javorfi, T., Erostyak, J., Gal, J., Buzady, A., Menczel, L., Grab, G., et al. (2006). Quantitative spectrophotometry using integrating cavities. *Journal of Photochemistry and Photobiology B: Biology, 82*, 127–131.

Jeans, C., Singer, S. W., Chan, C. S., VerBerkmoes, N. C., Shah, M., Hettich, R. L., et al. (2008). Cytochrome 572 is a conspicuous membrane protein with iron oxidation activity purified directly from a natural acidophilic microbial community. *International Society for Microbial Ecology Journal, 2*, 542–550.

Johnson, D. B., Kanao, T., & Hedrich, S. (2012). Redox transformations of iron at extremely low pH: Fundamental and applied aspects. *Frontiers in Microbiology, 3*, 96.

Kai, M., Yano, T., Tamegai, H., Fukumori, Y., & Yamanaka, T. (1992). *Thiobacillus ferrooxidans* cytochrome c oxidase: Purification, and molecular and enzymatic features. *Journal of Biochemistry, 112*, 816–821.

Kirk, J. T. O. (1997). Point-source integrating-cavity absorption meter: Theoretical principles and numerical modeling. *Applied Optics, 36*, 6123–6128.

Kucera, J., Bouchal, P., Lochman, J., Potesil, D., Janiczek, O., Zdrahal, Z., et al. (2013). Ferrous iron oxidation by sulfur-oxidizing *Acidithiobacillus ferrooxidans* and analysis of the process at the levels of transcription and protein synthesis. *Antonie Van Leeuwenhoek, 103*, 905–919.

Li, T. F., Painter, R. G., Ban, B., & Blake, R. C., II (2015). The multicenter aerobic iron respiratory chain of *Acidithiobacillus ferrooxidans* functions as an ensemble with a single macroscopic rate constant. *Journal of Biological Chemistry, 290*, 18293–18303.

Lubben, M., & Morand, K. (1994). Novel prenylated hemes as cofactors of cytochrome oxidases. *Journal of Biological Chemistry, 269*, 21473–21479.

Melin, F., Xie, H., Meyer, T., Ahn, Y. O., Gennis, R. B., Michel, H., et al. (2016). The unusual redox properties of C-type oxidases. *Biochimica et Biophysica Acta, 1857*, 1892–1899.

Merzlyak, M. N., & Naqvi, K. R. (2000). On recording the true absorption spectrum and the scattering spectrum of a turbid sample: Application to cell suspensions of the cyanobacterium *Anabaena variabilis*. *Journal of Photochemistry and Photobiology B: Biology, 58*, 123–129.

Meschi, F., Wiertz, F., Klauss, L., Blok, A., Ludwig, B., Merli, A., et al. (2011). Efficient electron transfer in a protein network lacking specific interactions. *Journal of the American Chemical Society, 133*, 16861–16867.

Monod, J. (1949). The growth of bacterial cultures. *Annual Reviews of Microbiology, 3*, 371–394.

Myers, J. M., & Myers, C. R. (2001). Role for outer membrane cytochromes OmcA and OmcB of *Shewanella putrefaciens* MR-1 in reduction of manganese dioxide. *Applied and Environmental Microbiology, 67*, 260–269.

Paquete, C. M., & Louro, R. O. (2014). Unveiling the details of electron transfer in multicenter redox proteins. *Accounts of Chemical Research, 47*, 56–65.

Paquete, C. M., Saraiva, I. H., Calcada, E., & Louro, R. O. (2010). Molecular basis for directional electron transfer. *Journal of Biological Chemistry, 285*, 10370–10375.

Pope, R. M., Weidermann, A. D., & Fry, E. S. (2000). Integrating cavity absorption meter measurements of dissolved substances and suspended particles in ocean water. *Dynamics of Atmospheres and Oceans, 31*, 307–320.

Quaranta, M., Borisov, S. M., & Klimant, I. (2012). Indicators for optical oxygen sensors. *Bioanalytical Reviews, 4*, 115–157.

Quatrini, R., Appia-Ayme, C., Denis, Y., Jedlicki, E., Holmes, D. S., & Bonnefoy, V. (2009). Extending the models for iron and sulfur oxidation in the extreme acidophile *Acidithiobacillus ferrooxidans*. *BMC Genomics, 10*, 394.

Quatrini, R., Appia-Ayme, C., Denis, Y., Ratouchniak, J., Veloso, F., Valdes, J., et al. (2006). Insights into the iron and sulfur energetic metabolism of *Acidithiobacillus ferrooxidans* by microarray transcriptome profiling. *Hydrometallurgy, 83*, 263–272.

Ram, R. J., VerBerkmoes, N., Thelen, M. P., Tyson, G. W., Baker, B. J., Blake, R. C., II, et al. (2005). Community proteomics of a natural microbial biofilm. *Science, 308*, 1915–1920.

Rana, N., McLean, S., Mann, B. E., & Poole, R. K. (2014). Interaction of the carbon monoxide-releasing molecule $Ru(CO)_3Cl$(glycinate) (CORM-3) with *Salmonella enterica* serovar typhimurium: *In situ* measurements of CO binding by integrating cavity dual beam spectrophotometry. *Microbiology, 160*, 2771–2779.

Rawlings, D. E. (2002). Heavy metal mining using microbes. *Annual Reviews of Microbiology, 56*, 65–91.

Rosenthal, D., & Cooper, D. Y. (1967). Methods of determining the photochemical action spectrum. *Methods in Enzymology, 10*, 616–629.

Sara, M., & Sleytr, U. B. (2000). S-layer proteins. *Journal of Bacteriology, 182*, 859–868.

Schafer, G. (1996). Bioenergetics of the archaebacterium *Sulfolobus*. *Biochimica et Biophysica Acta, 1277*, 163–200.

Schafer, G., Purschkee, W., & Schmidt, C. L. (1996). On the origin of respiration: Electron transport proteins from archaea to man. *FEMS Microbiology Reviews, 18*, 173–188.

Shibata, K., Benson, A. A., & Calvin, M. (1954). The absorption spectra of suspensions of living microorganisms. *Biochimica et Biophysica Acta, 15*, 461–470.

Shi, L., Chen, B., Wang, Z., Elias, D. A., Mayer, M. U., Gorby, Y. A., et al. (2006). Isolation of a high-affinity functional protein complex between OmcA and MtrC: Two outer membrane decaheme *c*-type cytochromes of *Shewanella oneidenis* MR-1. *Journal of Bacteriology, 188*, 4705–4714.

Singer, S. W., Chan, C. S., Zemla, A., VerBerkmoes, N. C., Hwang, M., Hettlich, R. L., et al. (2008). Characterization of cytochrome 579, an unusual cytochrome isolated from an iron-oxidizing microbial community. *Applied and Environmental Microbiology, 74*, 4454–4462.

Sleytr, U. B., & Beveridge, T. J. (1999). Bacterial S-layers. *Trends in Microbiology, 7*, 253–260.

Sousa, F. L., Alves, R. J., Pereira-Leal, J. B., Teixeira, M., & Pereira, M. M. (2011). A bioinformatics classifier and database for heme-copper oxygen reductases. *PLoS One, 6*, e19117.

Stock, J. B., Rauch, B., & Roseman, S. (1977). Periplasmic space in *Salmonella typhimurium* and *Escherichia coli*. *Journal of Biological Chemistry, 252*, 7850–7861.

Sugio, T., Ako, A., & Takeuchi, F. (2010). Sulfite oxidation catalyzed by aa_3-type cytochrome *c* oxidase in *Acidithiobacillus ferrooxidans*. *Bioscience Biotechnology and Biochemistry, 74*, 2242–2247.

Tuovinen, O. H., & Kelly, D. P. (1972). Biology of *Thiobacillus ferrooxidans* in relation to the microbiological leaching of sulphide ores. *Zeitschrift fur allgemeine Mikrobiologie, 12*, 311–346.

Turner, R. C., & Miles, K. E. (1957). The ultraviolet absorption spectra of the ferric ion and its first hydrolysis product in aqueous solutions. *Canadian Journal of Chemistry, 35*, 1002–1009.

Valdes, J., Pedroso, I., Quatrini, R., Dodson, R. J., Tettelin, H., Blake, R., II, et al. (2008). *Acidithiobacillus ferrooxidans* metabolism: From genome sequence to industrial applications. *BMC Genomics, 9*, 597.

Veith, A., Klingl, A., Zolghadr, B., Lauber, K., Mentele, R., Lottspeich, F., et al. (2009). *Acidianus, Sulfolobus* and *Metallosphaera* surface layers: Structure, composition and gene expression. *Molecular Microbiology, 73*, 58–72.

Vera, M., Schippers, A., & Sand, W. (2013). Progress in bioleaching: Fundamentals and mechanisms of bacterial metal sulfide oxidation – part A. *Applied Microbiology and Biotechnology, 97*, 7529–7541.

Verissimo, A. F., Pereira, M. M., Melo, A. M. P., Hreggvidsson, G. O., Kristjansson, J. K., & Teixeira, M. (2007). A *ba*$_3$ oxygen reductase from the thermohalophilic bacterium *Rhodothermus marinus*. *FEMS Microbiology Letters, 269*, 41–47.

Walter, R. L., Ealick, S. E., Friedman, A. M., Blake, R. C., 2nd, Proctor, P., & Shoham, M. (1996). Multiple wavelength anomalous diffraction (MAD) crystal structure of rusticyanin, a highly oxidizing cupredoxin with extreme acid stability. *Journal of Molecular Biology, 263*, 730–751.

Watanabe, T., Kojima, H., Umezawa, K., Hori, C., Takasuka, T. E., Kato, Y., et al. (2019). Genomes of neutrophilic sulfur-oxidizing chemolithoautotrophs representing 9 proteobacterial species from 8 genera. *Frontiers in Microbiology, 10*, 316.

Watling, H. R. (2006). The bioleaching of sulphide minerals with emphasis on copper sulphides — a review. *Hydrometallurgy, 84*, 81–108.

Weber, K. A., Achenbach, L. A., & Coates, J. D. (2006). Microbes pumping iron: Anaerobic microbial iron oxidation and reduction. *Nature Reviews Microbiology, 4*, 752–764.

Wilson, D. F. (2004). Identifying oxygen sensors by their photochemical action spectra. *Methods in Enzymology, 381*, 690–704.

Yarzabal, A., Appia-Ayme, C., Ratouchniak, J., & Bonnefoy, V. (2004). Regulation of the expression of the *Acidithiobacillus ferrooxidans rus* operon encoding two cytochromes *c*, a cytochrome oxidase and rusticyanin. *Microbiology, 150*, 2113–2123.

Yarzabal, A., Brasseur, G., Ratouchniak, J., Lund, K., Lemesle-Meunier, D., DeMoss, J. A., et al. (2002). The high molecular weight cytochrome *c* Cyc2 of *Acidithiobacillus ferrooxidans* is an outer membrane protein. *Journal of Bacteriology, 184*, 313–317.

Zimmerman, B. H., Nitsche, C. I., Fee, J. A., Rusnak, F., & Munck, E. (1988). Properties of a copper-containing cytochrome *ba*$_3$: A second terminal oxidase from the extreme thermophile *Thermus thermophilus*. *Proceedings of the National Academy of Science, USA, 85*, 5779–5783.

Zimmerman, S. B., & Trach, S. O. (1991). Estimation of macromolecule concentrations and excluded volume effects for the cytoplasm of *Escherichia coli*. *Journal of Molecular Biology, 222*, 599–620.